

1 **Size-resolved Composition and Morphology of Particulate**
2 **Matter During the Southwest Monsoon in Metro Manila,**
3 **Philippines**
4

5 Melliza Templonuevo Cruz^{1,2}, Paola Angela Bañaga^{1,3}, Grace Betito³, Rachel A. Braun⁴, Connor
6 Stahl⁴, Mojtaba Azadi Aghdam⁴, Maria Obiminda Cambaliza^{1,3}, Hossein Dadashazar⁴, Miguel
7 Ricardo Hilario³, Genevieve Rose Lorenzo¹, Lin Ma⁴, Alexander B. MacDonald⁴, Preciosa
8 Corazon Pabroa⁵, John Robin Yee⁵, James Bernard Simpás^{1,3}, Armin Sorooshian^{4,6}

9

- 10 ¹Manila Observatory, Quezon City [+1011108](#), Philippines
11 ²Institute of Environmental Science and Meteorology, University of the Philippines, Diliman, Quezon City 1101,
12 Philippines
13 ³Department of Physics, School of Science and Engineering, Ateneo de Manila University, Quezon City [+1011108](#),
14 Philippines
15 ⁴Department of Chemical and Environmental Engineering, University of Arizona, Tucson, AZ, USA
16 ⁵Philippine Nuclear Research Institute, Commonwealth Avenue, Diliman, Quezon City 1101, Philippines
17 ⁶Department of Hydrology and Atmospheric Sciences, University of Arizona, Tucson, AZ, USA

18

19 *Correspondence to:* Melliza Templonuevo Cruz (liz@observatory.ph)

20

21 **Abstract**

22 This paper presents novel results from size-resolved particulate matter (PM) mass, composition,
23 and morphology measurements conducted during the 2018 Southwest Monsoon (SWM) season in
24 Metro Manila, Philippines. Micro-Orifice Uniform Deposit Impactors (MOUDIs) were used to
25 collect PM sample sets composed of size-resolved measurements at the following aerodynamic
26 cutpoint diameters (D_p): 18, 10, 5.6, 3.2, 1.8, 1.0, 0.56, 0.32, 0.18, 0.10, 0.056 μm . ~~that were~~Each
27 sample set was analyzed for ~~mass, morphology, black carbon (BC), and~~ composition of the water-
28 soluble fraction. Analysis for mass were done on two sample sets while black carbon (BC) and
29 morphology analysis were done on a single sample set. The bulk of the PM mass was between
30 0.18–1.0 μm with a dominant mode between 0.32–0.56 μm . Similarly, most of the black carbon
31 (BC) mass was found between 0.10–1.0 μm , peaking between 0.18–0.32 μm . These peaks are
32 located in the Greenfield Gap or the size range between 0.10–1.0 μm , where wet scavenging by
33 rain is relatively inefficient. Similarly, most of the black carbon (BC) mass was found between
34 0.10–1.0 μm (the so-called Greenfield gap), peaking between 0.18–0.32 μm , where wet
35 scavenging by rain is inefficient. In the range of 0.10 – 0.18 μm , BC constituted 78.1% of the
36 measured mass. Comparable contributions of BC (26.9%) and the water-soluble fraction (31.3%)
37 to total PM were observed and most of the unresolved mass, which in total amounted to 41.8%,
38 was for diameters exceeding 0.32 μm . The water-soluble ions and elements exhibited an average
39 combined concentration of 8.53 $\mu\text{g m}^{-3}$, with SO_4^{2-} , NH_4^+ , NO_3^- , Na^+ , and Cl^- as the major
40 contributors. Positive Matrix Factorization (PMF) was applied to identify the possible aerosol
41 sources and estimate their contribution to the water-soluble fraction of collected PM. The factor
42 with the highest contribution was attributed to “Aged/~~Transported~~” aerosol (48.0%) while “Sea
43 Salt” (22.5%) and “Combustion” emissions (18.7%) had comparable contributions.
44 “Vehicular/Resuspended Dust” (5.6%) as well as “Waste Processing” emissions (5.1%) were also
45 identified. Microscopy analysis highlighted the ubiquity of non-spherical particles regardless of
46 size, which is significant when considering calculations of parameters such as single scattering
47 albedo, asymmetry parameter, and extinction efficiency.

48 ~~Results of this work have implications for aerosol impacts on public health, visibility, and regional~~
49 ~~climate as each of these depend on physicochemical properties of particles as a function of size.~~

50 The significant influence from Aged/~~Transported~~ aerosol to Metro Manila during the SWM season
51 indicates that local sources in this megacity do not fully govern this coastal area’s aerosol

52 properties ~~and that PM in Southeast Asia can travel long distances regardless of the significant~~
53 ~~precipitation and potential wet scavenging that could occur~~. That the majority of the regional
54 aerosol mass burden is accounted for by BC and other insoluble components has important
55 downstream effects on the aerosol hygroscopic properties, which depend on composition. The
56 results are relevant for understanding the impacts of monsoonal features on size-resolved aerosol
57 properties, notably aqueous processing and wet scavenging. Finally, the results of this work
58 provide contextual data for future sampling campaigns in Southeast Asia such as the airborne
59 component of the Cloud, Aerosol, and Monsoon Processes Philippines Experiment (CAMP²Ex)
60 planned for the SWM season in 2019. ~~Aerosol characterization via remote sensing is notoriously~~
61 ~~difficult in Southeast Asia, which elevates the importance of datasets such as the one presented~~
62 ~~here.~~
63

64 **1. Introduction**

65

66 Ambient atmospheric aerosol particles impact human health, visibility, climate, and the
67 hydrological cycle. Major factors governing these behaviors, such as deposition fraction in the
68 respiratory system and activation into cloud condensation nuclei (CCN), include size and chemical
69 composition. Therefore, size-resolved measurements of ambient aerosol particles can lend
70 additional insights to the behaviors and implications of particulate matter (PM) in the atmosphere.
71 One region of interest for characterization of aerosols is Southeast Asia due to increasing
72 urbanization and the exposure of the population to a variety of aerosol sources, both natural and
73 anthropogenic (Hopke et al., 2008). However, use of space-borne remote-sensing instrumentation
74 presents a challenge for characterization of aerosol in this region, due to issues such as varying
75 terrain and cloud cover (Reid et al., 2013).

76 The Philippines represents a country in Southeast Asia with a developing economy, rapid
77 urbanization, old vehicular technology, and less stringent air quality regulations (e.g., Alas et al.,
78 2017). It is also highly sensitive to the effects of climate change including prolonged dry periods
79 and reductions in southwest monsoon (SWM) rainfall in recent decades (e.g., Cruz et al., 2013).
80 Metro Manila is the country's capital and center of political and economic activities. Also referred
81 to as the National Capital Region, Metro Manila is composed of 16 cities and a municipality that
82 collectively occupy a land area of ~619 km². As of 2015, Metro Manila had a population of
83 approximately 12.88 million (Philippine Statistics Authority, 2015). Of the cities comprising the
84 Metro Manila area, the one that is the focus of this study, Quezon City, is the most populated (2.94
85 million people) with a population density of ~17,000 km⁻² as of 2015 (Philippine Statistics
86 Authority, 2015).

87 The rainfall pattern in Southeast Asia is governed by topographic effects and the prevailing
88 surface winds brought by the monsoons. Mountain ranges in the Philippines are generally oriented
89 north to south in the eastern and western coasts. As such, northeasterly winds during the East Asian
90 winter monsoon that starts in November brings wetness (dryness) on the eastern (western) coasts
91 of the country. In contrast, the rainy season starts in May when the Western North Pacific
92 subtropical high moves northeast and the Asian summer monsoon enables the propagation of
93 southwesterly wind through the Philippines (Villafuerte et al., 2014). Metro Manila, located on
94 the western side of the Philippines, therefore experiences wet (May-October) and dry (November-
95 April) seasons. The large seasonal shift in prevailing wind directions can cause changes in the

96 source locations of aerosol transported to the Philippines and the subsequent direction in which
97 emissions from the Philippines are transported, such as to the northwest (e.g., Chuang et al., 2013)
98 or southwest (e.g., Farren et al., 2019). However, one interesting feature of Metro Manila is the
99 consistency of $PM_{2.5}/PM_{10}$ mass concentrations during both the dry ($44/54 \mu\text{g m}^{-3}$) and wet seasons
100 ($43/55 \mu\text{g m}^{-3}$) (Kim Oanh et al., 2006), which stands in contrast to typical assumptions that
101 increased wet scavenging during rainy seasons would lead to decreases in measured PM (e.g., Liao
102 et al., 2006). While similar results are observed in Chennai, India, this behavior is different than
103 other cities in Asia, including Bandung City (Indonesia), Bangkok (Thailand), Beijing (China),
104 and Hanoi City (Vietnam), ~~that~~ which exhibit reduced $PM_{2.5}$ levels during the wet season as
105 compared to the dry season (Kim Oanh et al., 2006). While the total PM levels may stay constant
106 across the wet and dry seasons, seasonally-resolved analyses will provide additional insights into
107 how the composition, morphology, and sources (transported vs. local emissions) change on a
108 seasonal basis.

109 Metro Manila has been drawing growing interest for PM research owing to the significant
110 levels of black carbon (BC). A large fraction of PM in Metro Manila can be attributed to BC (e.g.,
111 $\sim 50\%$ of $PM_{2.5}$; Kim Oanh et al., 2006), with previously measured average values of BC at the
112 Manila Observatory (MO) reaching $\sim 10 \mu\text{g m}^{-3}$ for $PM_{2.5}$ (Simpas et al., 2014). The impacts of the
113 high levels of BC present on human health have also received attention (Kecorius et al., 2019).
114 Identified major sources of BC include vehicular, industrial, and cooking emissions (Bautista et
115 al., 2014; Kecorius et al., 2017). Vehicular emissions, especially along roadways where personal
116 cars and motorcycles, commercial trucks, and motorized public transportation, including powered
117 tricycles and *jeepneys*, are plentiful. For instance, measurements of $PM_{2.5}$ at the National Printing
118 Office (NPO) located alongside the major thoroughfare Epifanio de los Santos Avenue (EDSA)
119 were on average $72 \mu\text{g m}^{-3}$; this value is twice the average concentration at the Manila Observatory
120 (MO), an urban mixed site located approximately 5 km from NPO (Simpas et al., 2014). In
121 addition to local emissions, long-range transport of pollution, such as biomass burning, can also
122 impact the study region (e.g., Xian et al., 2013; Reid et al., 2016a/b). However, most past work
123 referenced above has focused on either total $PM_{2.5}$ or PM_{10} composition, and therefore, detailed
124 size-resolved composition information has been lacking in this region. Like other monsoonal
125 regions (Crosbie et al., 2015; Qu et al., 2015), it is of interest for instance to know if products of
126 aqueous processing (e.g., sulfate, organic acids) during the monsoonal period, promoted by the

127 high humidity, become more prominent in certain size ranges to ultimately enhance
128 hygroscopicity, which is otherwise suppressed with higher BC influence.

129 A year-long sampling campaign (Cloud, Aerosol, and Monsoon Processes Philippines
130 Experiment (CAMP²Ex) weatHER and CompoSition Monitoring (CHECSM) study) was
131 established in July 2018 to collect size-resolved aerosol measurements in Metro Manila. The aim
132 of this study is to report size-resolved PM measurements taken over the course of the SWM (July-
133 October) of 2018 in Quezon City, Metro Manila, Philippines as part of CHECSM. The results of
134 this study are important for the following reasons: (i) they provide size-resolved analysis of BC in
135 an area previously characterized as having one of the highest BC mass percentages in the whole
136 world; (ii) they provide a basis for better understanding the unusual phenomenon of having similar
137 PM levels during a wet and dry season; (iii) they provide contextual data for contrasting with both
138 other coastal megacities and also other monsoonal regions; and (iv) they can lend insights into the
139 characteristics of aerosol transported both into and out of Metro Manila and how important local
140 sources are in Metro Manila relative to transported pollution.

141 Outcomes of this study include (i) the first size-resolved characterization of both aerosol
142 composition and morphology in Metro Manila for the SWM, with implications in terms of PM
143 effects on climate, visibility, the hydrological cycle, and public health owing to the dependence of
144 these impacts on particle size; (ii) archival data that contributes to the timeline of aerosol research
145 in Metro Manila, and more broadly Southeast Asia, where there is considerable concern over air
146 pollution; and (iii) baseline data for aerosol composition to be used to inform and assist research
147 to be conducted during future field campaigns in Southeast Asia including the same seasonal
148 period (i.e., SWM) in 2019 as part of CAMP²Ex, which will involve both surface and airborne
149 measurements.

150 **2. Experimental Methods**

151 **2.1 Sample Site**

152 Sampling was performed at MO in Quezon City, Philippines (14.64° N, 121.08° E). ~~The~~
153 ~~sampling instrumentation was located~~Two MOUDI^s were placed ~~-inside an unoccupied room~~ on
154 the 3rd floor of the MO ~~office-administration~~ building (~85-87 m above sea level). ~~The inlet,~~
155 ~~located just outside the window, consists of a 2 m long stainless steel tube and a reducer and a~~
156 ~~reducer that is connected directly to the MOUDI inlet.~~ Figure 1 visually shows the sampling

157 location and potential surrounding [aerosol](#) sources. Past work focused on PM_{2.5} suggested that the
158 study location is impacted locally mostly by traffic, various forms of industrial activity, meat
159 cooking from local eateries, and, based on the season, biomass burning (Cohen et al., 2009). [This](#)
160 [is consistent with another source apportionment study which reported that potential sources in six](#)
161 [sites across Metro Manila include traffic, secondary particles, and biomass burning \(Kim Oanh et](#)
162 [al., 2013\).](#) ~~Fourteen sample sets were collected during the SWM season (July–October 2018), with~~
163 ~~details about the operational and meteorological conditions during each sample set shown in Table~~
164 ~~1.~~

165 Meteorological data were collected using a Davis Vantage Pro 2 Plus weather station ~~eo-~~
166 ~~located with the aerosol measurements at~~ [located on the roof \(~90 m above sea level, ~15 m above](#)
167 [ground level\) above where the MOUDIs were located](#) ~~MO~~. Except for precipitation, which is
168 reported here as accumulated rainfall, reported values for each meteorological parameter represent
169 averages for the sampling duration of each aerosol measurement.

170 ———The mean temperature during the periods of MOUDI sample collection ranged from
171 24.9 to 28.1° C, with accumulated rainfall ranging widely from no rain to up to 78.4 mm. To
172 identify sources impacting PM via long-range transport to the Metro Manila region, Figure
173 1a summarizes the five-day back-trajectories for air masses arriving at MO on the days when
174 samples were being collected, calculated using the NOAA Hybrid Single-Particle Lagrangian
175 Integrated Trajectory (HYSPLIT) model (Stein et al., 2015; Rolph, 2016). Trajectory calculations
176 were started at 00, 06, 12, and 18 hours in MO at the height of the MOUDI inlet ([~ 12 m above](#)
177 [ground level](#)) using meteorological files from the NCEP/NCAR Reanalysis dataset. Trajectory
178 cluster analysis was conducted using TrajStat (Wang et al., 2009). The back-trajectories in Figure
179 1a show that indeed 66% of the wind came from the southwest during the sampling periods.

180 **2.2 MOUDI Sample Sets**

181 ~~Particulate matter~~ [PM](#) was collected on Teflon substrates (PTFE membrane, 2 µm pore,
182 46.2 mm, Whatman) in Micro-Orifice Uniform Deposit Impactors (MOUDI, MSP Corporation,
183 Marple et al., 2014). Size-resolved measurements were taken at the following aerodynamic
184 cutpoint diameters (D_p): 18, 10, 5.6, 3.2, 1.8, 1.0, 0.56, 0.32, 0.18, 0.10, 0.056 µm. [Fourteen](#)
185 [sample sets were collected during the SWM season \(July–October 2018\), with details about the](#)
186 [operational and meteorological conditions during each sample set shown in Table 1. To determine](#)

187 [the optimum sampling time that will collect enough sample for subsequent analyses, collection](#)
188 [time for the first four samples ranged from 24 to 119 hours. Subsequent sampling were then fixed](#)
189 [to 48 hours with one sample set collected every week. The sampling collection was designed to](#)
190 [include samples from each day of the week so the collection cycled between Monday –](#)
191 [Wednesday, Tuesday – Thursday, Wednesday – Friday, and Saturday – Monday, starting at 1400](#)
192 [\(local time\) for the weekday samples and 0500 for the weekend samples. The Teflon substrates](#)
193 [were pretreated by washing with deionized water and air drying in a covered box. Substrates were](#)
194 [placed and retrieved from the cascade impactor inside the laboratory in an adjacent building and](#)
195 [transported to and from the sampling site using an impactor holder \(Csavina et al., 2011\). Samples](#)
196 [are immediately placed in the freezer upon retrieval.](#)

197 ~~For a subset of the sampling periods~~[On two occasions](#), two pairs of MOUDI sets ([Sets](#)
198 [MO3/MO4 and MO13/MO14](#)) were collected simultaneously such that ~~both sets~~[one set](#) in each
199 pair could undergo different types of analyses. [Sets 3 and 13](#) ~~One set in each pair~~ underwent
200 gravimetric analysis using a Sartorius ME5-F microbalance. [Substrates were conditioned for at](#)
201 [least 24 h at a mean temperature of 20-23 °C and a mean relative humidity of 30-40% before pre-](#)
202 [and post-weighing \(U.S. Environmental Protection Agency, 2016\).](#) MOUDI set 13 was
203 additionally examined with a Multi-wavelength Absorption Black Carbon Instrument (MABI;
204 Australian Nuclear Science and Technology Organisation). This optically-based instrument
205 quantifies absorption and mass concentrations at seven wavelengths between 405 and 1050 nm;
206 however, results are reported only for 870 nm to be consistent with other studies, as BC is the
207 predominant absorber at that wavelength (e.g., Ramachandran and Rajesh, 2007; Ran et al., 2016).
208 One additional sample set for microscopy analysis was collected for one hour on August 1 using
209 aluminum substrates.

210 **2.3 Chemical Composition Analysis**

211 [Twelve sample sets, composed of 11 samples each, were analyzed for water-soluble ions](#)
212 [and elements \(Table 2\).](#) In order to preserve samples for additional analysis, each Teflon substrate
213 was cut in half. A half of each substrate was extracted in 8 mL of Milli-Q water (18.2 MΩ-cm)
214 through sonication for 30 min in a sealed polypropylene vial. A blank substrate was processed in
215 the same method to serve as a background control sample. Subsequent chemical analysis of the
216 water-soluble components in the aqueous extracts were performed using ion chromatography (IC;

217 Thermo Scientific Dionex ICS - 2100 system) for the following species: cations = Na⁺, NH₄⁺,
218 Mg²⁺, Ca²⁺, dimethylamine (DMA), trimethylamine (TMA), diethylamine (DEA); anions =,
219 methanesulfonate (MSA), pyruvate, adipate, succinate, maleate, oxalate, phthalate, Cl⁻, NO₃⁻,
220 SO₄²⁻. Owing to co-elution of TMA and DEA in the IC system, a cumulative sum of the two is
221 reported here, which represents an underestimate of their total mass concentration owing to overlap
222 in parts of their peaks. Limits of detection (LOD) were calculated for each species based on their
223 respective calibration curve (Table S1), with LOD being three times the standard deviation of the
224 residuals (predicted signal minus measured signal) divided by the slope of the calibration curve
225 (Miller and Miller, 2018).

226 The aqueous extracts were simultaneously characterized for elemental composition using
227 triple quadrupole inductively coupled plasma mass spectrometry (ICP-QQQ; Agilent 8800 Series)
228 for the following species: K, Al, Fe, Mn, Ti, Ba, Zn, Cu, V, Ni, P, Cr, Co, As, Se, Rb, Sr, Y, Zr,
229 Nb, Mo, Ag, Cd, Sn, Cs, Hf, Tl, Pb. Limits of detection of the examined elements were calculated
230 automatically by the ICP-QQQ instrument and were in the ppt range (Table S1). The sample
231 concentrations represent an average of three separate measurements with a standard deviation of
232 3% or less.

233 Note that some species were detected by both IC and ICP-QQQ (i.e., Na⁺, K⁺, Mg²⁺, Ca²⁺),
234 and that the IC concentrations are used here for all repeated species with the exception of K⁺ owing
235 to better data quality from ICP-QQQ. All IC and ICP-QQQ species concentrations for samples
236 have been corrected by subtracting concentrations from background control samples. [For more](#)
237 [examples of the application of these methods used for substrate collection and IC/ICP analysis,](#)
238 [the reader is referred to other recent work \(Braun et al., 2017; Ma et al., 2019; Schlosser et al.,](#)
239 [2017\).](#)

240 **2.4 Microscopy Analysis**

241 As already noted, one MOUDI set on August 1 was devoted to microscopy analysis.
242 Morphology and additional elemental composition analysis was carried out on this set of aluminum
243 substrates using scanning electron microscopy equipped with energy dispersive X-ray
244 spectroscopy (SEM-EDX) in the Kuiper Imaging cores at the University of Arizona. Secondary
245 electron (SE) imaging and EDX elemental analysis were performed using a Hitachi S-4800 high
246 resolution SEM coupled to a Noran system Six X-ray Microanalysis System by Thermo Fisher

247 Scientific. EDX analysis on individual particles was performed with 30 kV accelerating voltage to
248 obtain weight percentages of individual elements. SEM-EDX results showed that the background
249 control aluminum substrate was dominated by Al (88.27%), with minor contributions from Ag
250 (5.34%), C (4.87%), O (0.79%), Fe (0.67%), and Co (0.05%). Such contributions were manually
251 subtracted from spectra of individual particles on sample substrates, with the remaining elements
252 scaled up to hundred percent. Image processing was conducted with Image J software to measure
253 particle dimensions and adjust the contrast and brightness of images to provide better visualization.

254 2.5 Computational Analysis

255 This study reports basic descriptive statistics for chemical concentrations and correlations
256 between different variables. Statistical significance hereafter corresponds to 95% significance
257 based on a two-tailed Student's t-test. To complement correlative analysis for identifying sources
258 of species, positive matrix factorization (PMF) modeling was carried out using the United States
259 Environmental Protection Agency's (US EPA) PMF version 5. A total of 132 samples from the 12
260 sets analyzed for water-soluble ions and elements were used in the PMF analysis. Species
261 concentrations were examined before being using as inputted to PMF. -Species considered as
262 "strong" based on high signal-to-noise ratios ($S/N > 1$) and those with at least 50% of the
263 concentrations above the ~~detection limit~~LOD were used in the PMF modeling (Norris et al., 2014).
264 This resulted in a 132 (samples) ~~xx~~ 30 (species) data matrix that was used as inputted to PMF.
265 Data points with concentrations exceeding the LOD had uncertainty quantified as ~~follows~~:

$$267 \sigma_{ij} = 0.05 \cdot X_{ij} + LOD_{ij}, \quad (\text{Equation 1})$$

268
269 where σ_{ij} , X_{ij} , and LOD_{ij} are the uncertainty, concentration, and LOD, respectively, of the j^{th}
270 species in the i^{th} sample (Reff et al., 2007). When concentration data were not available for a
271 particular stage of a MOUDI set for a species, the geometric mean of the concentrations for that
272 MOUDI stage and species was applied with uncertainty counted as four times the geometric mean
273 value (Polissar et al., 1998; Huang et al., 1999). A 25% extra modeling uncertainty was applied
274 to account for other sources of errors, such as changes in the source profiles and chemical
275 transformations (Dumanoglu et al., 2014; Norris et al., 2014). The model was run 20 times with a
276 randomly chosen starting point for each run.

277 3. Results

278 3.1 Total Mass Concentrations and Charge Balance

279 The average total mass concentration (\pm standard deviation) of water-soluble species across
280 all MOUDI stages (Table 1) during the study period was $8.53 \pm 4.48 \mu\text{g m}^{-3}$ (range = 2.7–16.6 μg
281 m^{-3}). The species contributing the most to the total water-soluble mass concentration during the
282 SWM included SO_4^{2-} ($44\% \pm 6\%$), NH_4^+ ($18\% \pm 5\%$), NO_3^- ($10 \pm 3\%$), Na^+ ($8 \pm 3\%$), and Cl^- (6%
283 $\pm 3\%$). The meteorological parameters from Table 1 best correlated to total water-soluble mass
284 concentrations were temperature ($r = 0.64$) and rainfall ($r = -0.49$). The highest total mass
285 concentration (set MO13/14 = $16.6 \mu\text{g m}^{-3}$) occurred during the period with one of the highest
286 average temperatures (27.8°C) and second least total rainfall (0.8 mm). Other sampling periods
287 with high mass concentrations (sets MO7, MO8, and MO12) coincided with the highest
288 temperature and lowest rainfall observations. High temperatures, and thus more incident solar
289 radiation, presumably enhanced production of secondary aerosol species via photochemical
290 reactions as has also been observed in other regions for their respective monsoon season (Youn et
291 al., 2013).

292 Low rainfall is thought to have been coincident with reduced wet scavenging of aerosol at
293 the study site as has been demonstrated for other regions such as North America (Tai et al., 2010)
294 and megacities such as Tehran (Crosbie et al., 2014). However, set MO11 exhibited a very low
295 concentration even with high temperature and lack of rainfall, which may be due to changes in the
296 source and transport of aerosol since this sample set coincided with a significant change in average
297 wind direction (290.2° for MO11 vs. $90.1^\circ - 127.5^\circ$ for all other MOUDI sets). While the reported
298 rainfall measurements were taken at MO, inhomogeneous rainfall patterns in the regions
299 surrounding the Philippines could also contribute to the wet scavenging of PM, thereby lowering
300 the quantity of transported particles reaching the sample site. Future work will address the
301 influence of spatiotemporal patterns of precipitation on PM loadings in the Philippines as a point
302 measurement at an aerosol observing site may be misleading.

303 On two occasions, two simultaneous MOUDI sets (Sets MO3/MO4 and MO13/MO14)
304 were collected for the potential to compare different properties that require separate substrates.
305 The total mass concentrations based on gravimetric analysis of sets MO3 and MO13 were $18.6 \mu\text{g}$
306 m^{-3} and $53.0 \mu\text{g m}^{-3}$, respectively (Figure 2). Both sets exhibited a dominant concentration mode
307 between $0.32\text{--}0.56 \mu\text{m}$ and the MO3 set was different in that it exhibited bimodal behavior with a

308 second peak between 1.8–3.2 μm . The sum of speciated water-soluble species accounted for only
309 27.8% and 31.3% of the total gravimetric mass of sets MO3 and MO13, respectively, indicative
310 of significant amounts of water-insoluble species undetected by IC and ICP-QQQ. When adding
311 the total mass of BC (14.3 $\mu\text{g m}^{-3}$) to the other resolved species from set MO13 (the one time BC
312 was measured), there was still 22.1 $\mu\text{g m}^{-3}$ of unresolved mass (41.8% of total PM). Most of the
313 unaccounted mass was for $D_p > 0.32 \mu\text{m}$.

314 The observation of BC accounting for 26.9% of total PM (14.3 $\mu\text{g m}^{-3}$) is consistent with
315 past work highlighting the significant fraction of BC in the ambient aerosol of Manila (Kim Oanh
316 et al., 2006; Bautista et al., 2014; Simpas et al., 2014; Kecorius et al., 2017). However, this fraction
317 of BC is very high compared to measurements during the monsoon season in other parts of the
318 world. The mass fraction of BC in total suspended PM (TSPM) was 1.6%/2.2% for the monsoon
319 season in 2013/2014 in Kadapa in southern India, even though the TSPM measured was
320 comparable to that in Manila (64.9 and 49.9 $\mu\text{g m}^{-3}$, for 2013 and 2014 in Kadapa, respectively)
321 (Begam et al., 2017). Multiple studies during the monsoon season in a coastal region in southwest
322 India showed BC mass contributions of 1.9 – 5% (Aswini et al., 2019 and references therein).
323 Airborne measurements around North America and in Asian outflow revealed that BC accounted
324 for only ~1-2% of $\text{PM}_{1.0}$ (Shingler et al., 2016) and ~5-15% of accumulation mode aerosol mass
325 (Clarke et al., 2004), respectively.

326 To investigate further about the missing species, a charge balance was carried out for all
327 MOUDI sets (Table 2) to compare the sum of charges for cations versus anions based on IC
328 analysis including K from ICP-QQQ analysis (species listed in Section 2.3). The slope of the
329 charge balances (cations on y-axis) for the cumulative dataset was 1.33 and ranged from 0.89 to
330 1.41 for the 12 individual MOUDI sets that had IC and ICP-QQQ analysis conducted on them.
331 Eleven of the 12 sets exhibited slopes above unity indicating that there was a deficit in the amount
332 of anions detected, which presumably included species such as carbonate and various organics. To
333 further determine if there were especially large anion or cation deficits in specific size ranges,
334 slopes are also reported for 0.056–1 μm and $> 1 \mu\text{m}$. There were no obvious differences other than
335 two MOUDI sets exhibited slopes below 1.0 for the smaller diameter range (0.056–1 μm) while
336 all slopes exceeded unity for $> 1 \mu\text{m}$.

337 3.2 Mass Size Distributions and Morphology

338 3.2.1 Black Carbon

339 The size-resolved nature of BC has not been characterized in Manila and MOUDI set
340 MO13 offered a view into its mass size distribution (Figure 3a). There was a pronounced peak
341 between 0.18–0.32 μm ($5.0 \mu\text{g m}^{-3}$), which is evident visually in the substrate's color when
342 compared to all other stages of that MOUDI set (Figure 3b). This observed peak in the mass size
343 distribution of BC is similar to previous studies of the outflow of East Asian countries (Shiraiwa
344 et al., 2008), biomass burning and urban emissions in Texas (Schwarz et al., 2008), measurements
345 in the Finnish Arctic (Raatikainen et al., 2015), and airborne measurements over Europe
346 (Reddington et al., 2013). In contrast, measurements in Uji, Japan showed a bimodal size
347 distribution for the mass concentration of BC in the submicrometer range (Hitzenberger and
348 Tohno, 2001).

349 In the present study, there were significant amounts of BC extending to as low as the 0.056-
350 0.1 μm MOUDI stage ($0.28 \mu\text{g m}^{-3}$) and extending up in the supermicrometer range, with up to
351 $0.25 \mu\text{g m}^{-3}$ measured between 1.8–3.2 μm . Remarkably, BC accounted for approximately 78.1%
352 (51.8%) by mass of the total PM in the range of 0.10 – 0.18 μm (0.18 – 0.32 μm). For comparison,
353 the mass percent contribution of BC measured in the megacity of Nanjing, China was 3.3% (1.6%)
354 at 0.12 (0.08) μm (Ma et al., 2017). Based on visual inspection of color on all MOUDI sets, MO13
355 appears to be representative of the other sets based on the relative intensity of the color black on
356 substrates with different cutpoint diameters (Figure 3b); the 0.18–0.32 μm substrate always was
357 the most black, with varying degrees of blackness extending consistently into the supermicrometer
358 stages.

359 Microscopy analysis revealed evidence of non-spherical particles in each MOUDI stage
360 below 1 μm (Figure 4), which is significant as the common assumption theoretically is that
361 submicrometer particles are typically spherical (e.g., Mielonen et al., 2011). Errors in this
362 assumption impact numerical modeling results and interpretation of remote sensing data for
363 aerosols (e.g., Kahnert et al., 2005), owing to incorrect calculations of parameters such as single
364 scattering albedo, asymmetry parameter, and extinction efficiency (e.g., Mishra et al., 2015). Some
365 studies have noted that submicrometer particles could be composed of an agglomeration of small
366 spherical particles originally formed through gas-to-particle conversion processes (Almeida et al.,
367 2019), which could potentially explain the appearance for some of the observed particles in Figure
368 4. Since only single particles were examined that may not be fully representative of all particles

369 on a particular MOUDI substrate, it is noteworthy that all five particles shown between 0.056 – 1
370 μm were irregularly shaped with signs of both multi-layering and constituents adhered to one
371 another.

372 The images show that a potentially important source of BC in the area could be soot
373 aggregates, which are formed by a vaporization-condensation process during combustion often
374 associated with vehicular exhaust (e.g., Chen et al., 2006; Chithra and Nagendra, 2013; Wu et al.,
375 2017). Kecorius et al. (2017) projected that 94% of total roadside refractory PM with number
376 concentration modes at 20 and 80 nm in the same study region was linked to *jeepneys*, the most
377 popular and inexpensive mode of public transport in Metro Manila. ~~with number concentration~~
378 ~~modes at 20 and 80 nm.~~ They associated the larger mode with soot agglomerates, which is
379 consistent with the smallest MOUDI size range examined here (0.056-0.1 μm ; Figure 4b)
380 exhibiting signs of agglomeration.

381 The total BC mass concentration integrated across all stages of MOUDI set MO13 (14.3
382 $\mu\text{g m}^{-3}$) was remarkably high in contrast to BC levels measured via either filters, aethalometers, or
383 single particle soot photometers in most other urban regions of the world (Metcalf et al., 2012 and
384 references therein): Los Angeles Basin (airborne: 0.002–0.53 $\mu\text{g m}^{-3}$), Atlanta, Georgia (ground:
385 0.5–3.0 $\mu\text{g m}^{-3}$), Mexico City (airborne: 0.276–1.1 $\mu\text{g m}^{-3}$), Sapporo, Japan (ground: 2.3–8.0 μg
386 m^{-3}), Beijing, China (ground: 6.3–11.1 $\mu\text{g m}^{-3}$), Bangalor, India (ground: 0.4–10.2 $\mu\text{g m}^{-3}$), Paris,
387 France (ground: 7.9 $\mu\text{g m}^{-3}$), Dushanbe, Russia (ground: 4–20 $\mu\text{g m}^{-3}$), Po Valley, Italy (ground:
388 0.5–1.5 $\mu\text{g m}^{-3}$), Thessaloniki, Greece (ground: 3.3–8.9 $\mu\text{g m}^{-3}$). This is intriguing in light of
389 extensive precipitation, and thus wet scavenging of PM, during the study period, which is offset
390 by enormous anthropogenic emissions in the region, such as by powered vehicles like the *jeepneys*
391 that are notorious for BC exhaust (Kecorius et al., 2017).

392 A possible explanation for the large contribution of BC to PM, and the persistence of PM
393 after rain events (Kim Oanh et al., 2006), is that the BC is not efficiently scavenged by precipitating
394 rain drops. Small particles enter rain drops via diffusion whereas large particles enter via
395 impaction. However, particles with a diameter in the range of 0.1–1 μm (known as the Greenfield
396 gap) are too large to diffuse efficiently and too small to impact, and are therefore not efficiently
397 scavenged (Seinfeld and Pandis, 2016). Absorption spectroscopy of set MO13 (Figure 2b) reveals
398 that 95% of the BC mass is concentrated in the Greenfield gap, and thus the removal of BC due to
399 precipitation is inefficient. The Greenfield gap contains $62 \pm 11\%$ of the total mass (calculated for

400 MO3/MO13) and $65 \pm 10\%$ of the water-soluble mass (calculated for the other 12 MO sets). [As](#)
401 [noted earlier, BC observations discussed in this paper were based only on a single MOUDI set and](#)
402 [the effect of inefficient scavenging in the Greenfield Gap could just be one of the many potential](#)
403 [processes affecting the BC mass size distribution. Subsequent work that will include BC](#)
404 [measurements in the dry season will further investigate this hypothesis.](#)

405 3.2.2 Water-Soluble Ions

406 There were two characteristic mass size distribution profiles for the water-soluble ions
407 speciated by IC₂ depending on whether the species were secondarily produced via gas-to-particle
408 conversion or associated with primarily emitted supermicrometer particles. The average IC species
409 mass concentration profile across all MOUDI sets is shown in Figure 5. ~~Secondarily-Secondarily-~~
410 produced species exhibited a mass concentration mode between 0.32–0.56 μm , including common
411 inorganic species (SO_4^{2-} , NH_4^+), MSA, amines (DMA, TMA+DEA), and a suite of organic acids,
412 such as oxalate, phthalate, succinate, and adipate, produced via precursor volatile organic
413 compounds (VOCs). Two organic acids with peaks in other size ranges included maleate (0.56–1
414 μm) and pyruvate (0.1–0.18 μm). Sources of the inorganics are well documented with SO_4^{2-} and
415 NH_4^+ produced by precursor vapors SO_2 and NH_3 , respectively, with ocean-emitted
416 dimethylsulfide (DMS) as an additional precursor to SO_4^{2-} and the primary precursor to MSA.

417 Precursors leading to ~~secondarily-secondarily-~~produced alkyl amines such as DMA, TMA,
418 and DEA likely originated from a combination of industrial activity, marine emissions, biomass
419 burning, vehicular activity, sewage treatment, waste incineration, and the food industry (e.g.,
420 Facchini et al., 2008; Sorooshian et al., 2009; Ge et al., 2011; VandenBoer et al., 2011); another
421 key source of these species, animal husbandry (Mosier et al., 1973; Schade and Crutzen, 1995;
422 Sorooshian et al., 2008), was ruled out owing to a scarcity of such activity in the study region.
423 ~~Secondarily-Secondarily-~~produced amine salts likely were formed with SO_4^{2-} as the chief anion
424 owing to its much higher concentrations relative to NO_3^- or organic acids.

425 Dimethylamine was the most abundant amine similar to other marine (Muller et al., 2009)
426 and urban regions (Youn et al., 2015); the average concentration of DMA integrated over all
427 MOUDI stages for all sample sets was 62.2 ng m^{-3} in contrast to 29.8 ng m^{-3} for TMA+DEA. For
428 reference, the other key cation (NH_4^+) participating in salt formation with acids such as H_2SO_4 and
429 HNO_3 was expectedly much more abundant ($1.64 \mu\text{g m}^{-3}$). With regard to the competitive uptake

430 of DMA versus NH_3 in particles, the molar ratio of $\text{DMA}:\text{NH}_4^+$ exhibited a unimodal profile
431 between 0.1–1.8 μm with a peak of 0.022 between 0.32–0.56 μm and the lowest values at the tails
432 (0.004 between 0.1–0.18 and 1–1.8 μm); DMA was not above detection limits for either $D_p < 0.1$
433 μm or $D_p > 1.8 \mu\text{m}$. The molar ratios observed were consistent with values measured in urban air
434 of Tucson, Arizona and coastal air in Marina, California (0–0.04; Youn et al., 2015) and near the
435 lower end of the range measured in rural and urban air masses sampled near Toronto (0.005–0.2:
436 VandenBoer et al., 2011).

437 The most abundant organic acid was oxalate ($195 \pm 144 \text{ ng m}^{-3}$), followed by succinate (21
438 $\pm 41 \text{ ng m}^{-3}$), phthalate ($19 \pm 25 \text{ ng m}^{-3}$), maleate ($17 \pm 15 \text{ ng m}^{-3}$), and adipate ($5 \pm 8 \text{ ng m}^{-3}$). The
439 observation of mass concentrations increasing with decreasing carbon number for dicarboxylic
440 acids (i.e., oxalate > succinate > adipate) is consistent with many past studies for other regions as
441 larger chain acids undergo oxidative decay to eventually form oxalate (e.g., Kawamura and
442 Ikushima, 1993; Kawamura and Sakaguchi, 1999; Sorooshian et al., 2007). Maleate is an
443 unsaturated dicarboxylic acid emitted from gas and diesel engines (Rogge et al., 1993) and a
444 product from the photo-oxidation of benzene (Kawamura and Ikushima, 1993). The aromatic
445 dicarboxylic acid phthalate is a known photo-oxidation product of naphthalene and stems largely
446 from plastic processing and fuel combustion (Fraser et al., 2003; Kautzman et al., 2010; Fu et al.,
447 2012; Kleindienst et al., 2012). The oxidation product (MSA) of ocean-derived DMS exhibited an
448 overall average concentration of $11 \pm 7 \text{ ng m}^{-3}$, which is near the lower end of the range of levels
449 reported in other coastal and marine environments (from undetected up to $\sim 200 \text{ ng m}^{-3}$) (e.g.,
450 Saltzman et al., 1983, 1986; Berresheim 1987; Watts et al., 1987; Burgermeister and Georgii,
451 1991; Sorooshian et al., 2015; Xu and Gao, 2015).

452 Water-soluble species exhibiting a peak in the supermicrometer range, usually between
453 1.8–5.6 μm , include those with known affiliations with sea salt (Na^+ , Cl^- , K^+ , Mg^{2+}) and crustal
454 materials such as dust (Ca^{2+}). Nitrate peaked between 1.8–3.2 μm , and was best correlated with
455 Na^+ and Mg^{2+} , suggestive of HNO_3 partitioning to sea salt as has been observed in other coastal
456 regions (e.g., Prabhakar et al., 2014a). There was very little NO_3^- in the submicrometer range (0.05
457 $\pm 0.04 \mu\text{g m}^{-3}$) in contrast to supermicrometer sizes ($0.78 \pm 0.47 \mu\text{g m}^{-3}$). More submicrometer
458 NO_3^- in the form of NH_4NO_3 would be expected if there was an excess of NH_3 after neutralizing
459 SO_4^{2-} . The mean ammonium-to-sulfate molar ratio for submicrometer sizes was 2.32 ± 0.52 (range:
460 1.11 – 2.78), with full neutralization of SO_4^{2-} in 10 of 12 MOUDI sets. Thus, there was a non-

461 negligible excess in NH_3 that presumably participated in salt formation with HNO_3 and organic
462 species. The significant levels of NO_3^- in the same mode as Na^+ and Cl^- contributed to the
463 significant Cl^- depletion observed, as the mean $\text{Cl}^-:\text{Na}^+$ mass ratio between 1-10 μm (i.e., range of
464 peak sea salt influence) was 0.81 ± 0.28 , which is much lower than the ratio for pure sea salt (1.81)
465 (Martens et al., 1973). The subject of Cl^- depletion in this region will be investigated more
466 thoroughly in subsequent work.

467 Figure 6 shows SEM images of representative single particles in each supermicrometer
468 stage. As would be expected for sea salt and crustal material, most of the particles shown are not
469 spherical. Interestingly, only the particle shown between 1–1.8 μm was close to being spherical.
470 Its composition based on EDX analysis was accounted for mostly by carbon (93.7%) with lower
471 amounts of oxygen (5.8%) and Fe (0.5%). Sea salt particles were found in the next two stages
472 owing to the highest combined weight percentages of Na^+ and Cl^- based on EDX analysis: 1.8–3.2
473 $\mu\text{m} = 36.9\%$; 3.2–5.6 $\mu\text{m} = 46.9\%$. The salt particles are not necessarily cubical but more rounded
474 with signs of agglomeration. These two particles were the only ones among the 11 MOUDI stages
475 exhibiting an EDX signal for S, with contributions amounting to $\sim 2\%$ in each particle. This may
476 be linked to natural SO_4^{2-} existing in sea salt particles. Also, the particle between 3.2–5.6 μm
477 contained a trace amount of Sc (1%). The largest three particles ($\geq 5.6 \mu\text{m}$) were expectedly
478 irregularly shaped with both sharp and rounded edges, comprised mostly of oxygen, Al, Fe, and
479 Ca based on EDX analysis.

480 3.2.3 Water-Soluble Elements

481 Averaged data across all MOUDI sets reveal that ICP-QQQ elements exhibited a variety
482 of mass concentration profiles ranging from a distinct mode in either the sub- or supermicrometer
483 range to having multiple modes below and above 1 μm (averages across all MOUDI sets shown
484 in Figure 7). There were several elements with only one distinct peak, being in one of the two
485 stages between 0.18-1.0 μm , including As, Cd, Co, Cr, Cs, Cu, Hf, Mn, Mo, Ni, Rb, Se, Sn, Tl, V,
486 Pb, and Zn. In contrast, the following elements exhibited only one distinct peak in the
487 supermicrometer range: Al, Ba, P, Sr, Ti, Y, and Zr. The rest of the elements exhibited more
488 complex behavior with two distinct peaks in the sub- and supermicrometer range (Ag, Fe, Nb).
489 The following section discusses relationships between all of the ions and elements with a view
490 towards identifying characteristic sources.

491 3.3 Characteristic Sources and Species Relationships

492 A combination of PMF and correlation analysis helped identify clusters of ~~closely~~ closely-
493 related species stemming from distinct sources. The ~~final~~ PMF solution ~~with five factors, based on~~
494 ~~five groups of species~~ (Figure 8); ~~was chosen because it~~ passed ~~the~~ criteria ~~of physical~~
495 ~~meaningfulness associated with being physically valid~~ and ~~it had a the close proximity of the~~
496 calculated ratio of $Q_{\text{true}}:Q_{\text{expected}}$ (1.2) ~~that was very close to the theoretical value of~~ 1.0. There
497 was a high coefficient of ~~variation-determination~~ between measured and predicted mass
498 concentration when summing up all species for each MOUDI stage ($r^2 = 0.79$; sample size, $n =$
499 132), which added confidence in relying on the PMF model for source apportionment of PM. The
500 five distinct clusters were named for their most plausible sources based on the species included in
501 the groupings, with their overall contributions to the total mass based on PMF analysis shown in
502 parenthesis (Table 3): Aged/~~Transported~~ (48.0%), Sea Salt (22.5%), Combustion (18.7%),
503 Vehicular/Resuspended Dust (5.6%), and Waste Processing (5.1%). For reference, a previous
504 study near the northwestern edge of the Philippines identified six source factors for PM_{2.5} that are
505 fairly similar to those here (Bagtasa et al., 2018): sea salt, resuspended fine dust, local solid waste
506 burning, and long range transport of (i) industrial emissions, (ii) solid waste burning, and (iii)
507 secondary sulfate. Each of our five groupings will be discussed in detail below in decreasing order
508 of contribution to total measured mass concentrations.

509 3.3.1 Aged/~~Transported~~ Aerosol

510 Although not due to one individual source, there was a distinct PMF factor that included
511 species commonly produced via gas-to-particle conversion processes (NH_4^+ , SO_4^{2-} , MSA,
512 oxalate). Correlation analysis (Table 4) also pointed to a large cluster of species significantly
513 related to each other, including the aforementioned ions and a suite of other organic acids
514 (phthalate, succinate, adipate), MSA, and DMA. The latter three inorganic and organic acid ions
515 exhibited significant correlations with each other ($r \geq 0.68$), but also with several elements ($r \geq$
516 0.36: K, V, Rb, Cs, Sn), which were likely co-emitted with the precursor vapors of the secondarily
517 produced ions. Although BC concentrations were quantified from set MO13 ~~only~~, ~~their~~
518 ~~interrelationships with water soluble ions from simultaneously collected set MO14 are~~
519 ~~representative for other sets.~~ The results showed that BC was significantly correlated ($r: 0.61-$
520 0.92) with 15 species, including those mentioned above (owing to co-emission) and also a few

521 elements that were found via PMF to be stronger contributors to the Combustion source discussed
522 in Section 3.3.3 (Ni, Cu, As, Se, Cd, Tl, Pb).

523 This PMF source factor is referred to as Aged Aerosol/Transported owing to its
524 characteristic species being linked to secondary particle formation from emissions of local and
525 regional sourcesources distant from the sample site. Examples include MSA and DMA being
526 secondarily produced from ocean-derived gaseous emissions (e.g., Sorooshian et al., 2009), and K
527 stemming from biomass burning emissions from upwind regions such as Sumatra and Borneo
528 (Xian et al., 2013). Previous studies (Reid et al., 2012; Wang et al., 2013) have shown that
529 phenomena such as SWM and El-Nino events not only influence biomass burning activities in the
530 Malay Peninsula but also impact the transport and distribution of emissions in the study region.
531 For instance, Reid et al. (2016b) showed that enhancement in monsoonal flow facilitates the
532 advection of biomass burning and anthropogenic emissions to the Philippines from Sumatra and
533 Borneo. Subsequent work will investigate more deeply the impact of biomass burning from those
534 upwind regions on the sample site during the SWM.

535 While NH_4^+ and SO_4^{2-} require time for production owing to being secondarily-secondarily-
536 produced from precursor vapors (i.e., SO_2 , NH_3), oxalate is the smallest dicarboxylic acid and
537 requires lengthier chemistry pathways for its production and thus is more likely produced in
538 instances of aerosol transport and aging (e.g., Wonaschuetz et al., 2012; Ervens et al., 2018). The
539 various elements associated with this cluster are co-emitted with the precursors to the
540 aforementioned ions and are linked to a variety of sources: metallurgical processes (Anderson et
541 al., 1988; Csavina et al., 2011; Youn et al., 2016), fuel combustion (Nriagu, 1989; Allen et al.,
542 2001; Shafer et al., 2012; Rocha and Correa, 2018), residual oil combustion (Watson et al., 2004),
543 biomass burning (Maudlin et al., 2015), marine and terrestrial biogenic emissions (Sorooshian et
544 al., 2015), and plastics processing (Fraser et al., 2003). In addition, there is extensive ship traffic
545 in the general study region, which is a major source of species in this cluster of species, particularly
546 V and SO_4^{2-} (e.g., Murphy et al., 2009; Coggon et al., 2012).

547 PMF analysis suggested that the Aged Aerosol/Transported factor contributed 48.0% to
548 the total water-soluble mass budget during the study period. Most of the contribution resided in
549 the submicrometer range (68.9%) unlike the supermicrometer range (18.6%), which is consistent
550 with the overall mass size distribution of total PM peaking in the submicrometer range (Figure 2).
551 The reconstructed mass size distribution for this PMF source factor shows the dominance of the

552 mass in the submicrometer range with a peak between 0.32–0.56 μm (Figure 9). The correlation
553 matrices for the sub- and supermicrometer size ranges also show that the correlations between the
554 species most prominent in the Aged ~~Aerosol/Transported~~ category are stronger for the former size
555 range (Tables S2-S3). The contribution of this PMF factor to the supermicrometer range is likely
556 associated with species secondarily produced on coarse aerosol such as dust and sea salt. This is
557 evident in the individual species mass size distributions where there is a dominant submicrometer
558 mode but also non-negligible mass above 1 μm .

559 Even though the PM in a heavily populated urban region, such as Metro Manila, is typically
560 thought to be dominated by local sources of aerosols, the current PMF results show that ~~the largest~~
561 ~~contributions to water soluble aerosol mass are from Aged/Transported pollution.~~
562 ~~contribution from long range transport is still discernible.~~ This finding is contrary to the expectation that (a) the
563 signal of transported aerosols would be lost in the noise of locally-produced aerosols, ~~and (b) the~~
564 ~~removal of aerosols over the ocean surrounding the Philippines by processes such as wet~~
565 ~~scavenging would significantly reduce the contribution of transported aerosols.~~ Even though other
566 ~~cities may have different pollution signatures, varying in pollutant type and amount, this~~
567 ~~phenomenon of Aged/Transported pollution forming a significant portion of the water soluble~~
568 ~~mass may be applicable to other cities, especially those in Southeast Asia.~~

569 3.3.2 Sea Salt

570 As the MO sampling site is approximately 13 km from the nearest shoreline (Figure 1a)
571 and downwind of Manila Bay in the SWM season, there was a great potential for marine emissions
572 to impact the samples. There were several species with similar mass size distributions (mode: 1.8–
573 5.6 μm) and highly correlated total mass concentrations ($r \geq 0.51$) that are linked to sea salt: Cl,
574 Na⁺, Ca²⁺, Mg²⁺, Ba, and Sr. The correlations between these species were stronger when examining
575 just the supermicrometer range as compared to the submicrometer range (Tables S2-S3). The
576 majority of these species was used in PMF analysis and formed a distinct cluster amounting to
577 22.0% of the total study period's mass budget. This source contributed only 0.6% to the
578 submicrometer mass concentration but 53.5% for the supermicrometer size range. The
579 reconstructed mass size distribution for this source factor is shifted farthest to the larger diameters
580 as compared to the other four sources with a peak between 1.8-3.2 μm (Figure 9).

581 It is noteworthy that this factor has the highest share of NO_3^- among all identified sources.
582 This result is consistent with mass size distributions shown in Figure 5 in which NO_3^- peaks in the
583 supermicrometer range similar to sea salt constituents (e.g., Na^+ and Cl^-). Although sea salt
584 particles naturally contain NO_3^- (Seinfeld and Pandis, 2016) (mass ratio of $\text{NO}_3^-:\text{Na}^+ = 9.8 \times 10^{-8}$
585 $- 6.5 \times 10^{-5}$), the extremely high ratio of $\text{NO}_3^-:\text{Na}^+$ (mass ratio ~ 1.8) suggests that only a negligible
586 portion of NO_3^- in this factor originated from primary sea salt particles. Thus, the majority of NO_3^-
587 is most likely due to HNO_3 partitioning to existing sea salt particles (e.g., Fitzgerald, 1991; Allen
588 et al., 1996; Dasgupta et al., 2007; Maudlin et al., 2015). In addition, the $\text{Cl}^-:\text{Na}^+$ mass ratio in this
589 profile (0.65) is smaller than that in sea salt particles (1.81), indicating high Cl^- depletion mainly
590 due to reactions of HNO_3 with NaCl (Ro et al., 2001; Yao et al., 2003; Braun et al., 2017).
591 Moreover, elevated loadings of trace elements (e.g., Ba, Cu, Zn, and Co) could be linked to mixing
592 of marine emissions with urban sources (e.g., vehicle and industrial emissions) during their
593 transport inland to the sampling site (Roth and Okada, 1998). This process of aging is consistent
594 with the observed morphology of the sea salt particles in this study, revealing non-cubical shapes
595 that are rounded owing to the likely addition of acidic species such as HNO_3 (Figure 6).

596 3.3.3 Combustion

597 There are numerous sources of combustion in the study region, including a variety of
598 mobile sources (e.g., cars, utility vehicles, trucks, buses, motorcycles) and stationary sources (e.g.,
599 power stations, cement works, oil refineries, boiler stations, utility boilers). Consequently, the next
600 highest contributor to total mass during the study period according to PMF (18.7%) was the cluster
601 of species including Ni, As, Co, P, Mo, and Cr, which is defined as the Combustion factor. These
602 species have been reported to be rich in particles emitted from combustion of fossil fuel and
603 residual oil (Linak and Miller, 2000; Allen et al., 2001; Wasson et al., 2005; Mahowald et al.,
604 2008; Mooibroek et al., 2011; Prabhakar et al., 2014b). Although not included in PMF analysis,
605 other species significantly correlated with the previous ones include maleate and Ag, which also
606 stem from fuel combustion (Kawamura and Kaplan, 1987; Lin et al., 2005; Sorooshian et al.,
607 2007). Ag specifically is an element in waste incinerator fly ash (Buchholz and Landsberger, 1993;
608 Tsakalou et al., 2018) and its strong correlation with Co ($r = 0.85$) and Mo ($r = 0.64$) provides
609 support for this source factor being linked to combustion processes. Maleate is commonly found
610 in engine exhaust (Kawamura and Kaplan, 1987), while Cr is a tracer for power plant emissions

611 (Singh et al., 2002; Behera et al., 2015). Of all species examined in this study, BC was best
612 correlated with As ($r = 0.92$), while its correlation with Ni ($r = 0.85$) was among the highest.

613 As the elements in this cluster peaked in concentration in the submicrometer mode, the
614 weight percentage of this factor is more than double below $1\ \mu\text{m}$ (23.9%) as compared to above 1
615 μm (11.3%). The reconstructed mass size distribution for this source factor peaks between 0.18 –
616 $0.32\ \mu\text{m}$, which is smaller than the modal diameter range for the Aged/~~Transported~~ source factor
617 (0.32 – $0.56\ \mu\text{m}$) likely owing to closer sources and thus less time for growth to occur via
618 condensation and coagulation.

619 **3.3.4 Vehicular/Resuspended Dust**

620 The next PMF source factor contains chemical signatures of dust because of high
621 contributions to Al, Ti, Ca, and Fe. These crustal elements are strongly related to resuspension of
622 dust by traffic and construction activities (Singh et al., 2002; Harrison et al., 2011). Other elements
623 that were prominent in this factor included Zr, Y, Mn, Cr, and Ba, which are associated with tire
624 and brake wear (Adachi and Tainosho, 2004; Gietl et al., 2010; Song and Gao, 2011; Harrison et
625 al., 2012; Vossler et al., 2016), although some of them can be linked to ~~the~~ exhaust as well (e.g.,
626 Lin et al., 2005; Song and Gao, 2011). This source is named Vehicular/Resuspended Dust and
627 contributed 5.6% to the total study period's mass concentrations.

628 The weight percentage contribution of this factor was much higher for the supermicrometer
629 range (11.3%) as compared to the submicrometer range (1.5%), which is consistent with the Sea
630 Salt source factor owing to similar mass size distributions of the individual species associated with
631 the two source categories (Figures 5 and 7). Additional species correlated significantly with the
632 crustal species included Hf and Nb, which also exhibited mass peaks between 1.8 – $3.2\ \mu\text{m}$. The
633 reconstructed mass size distribution for this source factor is similar to that of Sea Salt in that there
634 is a peak between 1.8 – $3.2\ \mu\text{m}$, but there is less of a unimodal profile owing to what appears to be
635 a secondary mode between 0.56 – $1.0\ \mu\text{m}$ (Figure 9), which could be linked to some of the non-dust
636 components of vehicular emissions.

637 **3.3.5 Waste Processing**

638 The final PMF source factor, contributing the least overall to total mass (5.1%), featured
639 Zn, Cd, Pb, Mn, and Cu as its main components. These species are linked to waste processing,

640 including especially electronic waste (e-waste) and battery burning and recycling (Gullett et al.,
641 2007; Iijima et al., 2007), which was previously reported for Manila (Pabroa et al., 2011). The
642 latter study reported that although there are a few licensed operations for battery recycling, there
643 are numerous unregulated cottage melters across Manila that regularly melt metal from batteries
644 and discard the waste freely. Fujimori et al. (2012) additionally showed that e-waste recycling led
645 to emissions of the following elements (in agreement with this PMF cluster) around Metro Manila:
646 Ni, Cu, Pb, Zn, Cd, Ag, In, As, Co, Fe, and Mn.

647 This was the only PMF factor exhibiting comparable weight percentages both below
648 (5.1%) and above 1 μm (5.3%). This is reflected in the mass size distributions of the species
649 included in this cluster being fairly uniformly distributed below and above 1 μm . This is also
650 demonstrated in the reconstructed mass size distribution of this source factor as it clearly exhibits
651 a mode between the other four sources (0.56–1.0 μm) and is the broadest mode (Figure 9). The
652 explanation for this is likely rooted in the diversity of sources contained within this source profile
653 that lead to different sizes of particles. Examples of such sources include processing of different
654 types of waste at varying temperatures and through various processes (e.g., burning, melting,
655 grinding) (Keshtkar and Ashbaugh, 2007),

656 4. Conclusions

657 This study used various analytical techniques (gravimetry, [ion chromatography](#), [triple](#)
658 [quadrupole inductively coupled plasma mass spectrometry](#)~~ICP-MS~~, black carbon spectroscopy,
659 and microscopy), meteorological data, and a source apportionment model ([Positive Matrix](#)
660 [Factorization](#)) to characterize the sources, chemical composition, and morphology of size-resolved
661 ambient [particulate matter \(PM\) collected using Micro-Orifice Uniform Deposit Impactors](#)
662 [\(MOUDIs\)](#) in Metro Manila, Philippines during the [southwest monsoon season \(SWM\)](#) season of
663 2018. The main results of this study include the following:

- 664
- 665 • The total mass concentrations were measured on two occasions and were $18.6 \mu\text{g m}^{-3}$ and 53.0
666 $\mu\text{g m}^{-3}$. Water-soluble mass concentrations were measured on 12 occasions and were on
667 average $8.53 \pm 4.48 \mu\text{g m}^{-3}$ (range = $2.7\text{--}16.6 \mu\text{g m}^{-3}$). Simultaneous measurements of total,
668 water-soluble, and [black carbon \(BC\)](#) mass revealed a composition of 26.9% BC, 31.3% water-
669 soluble components, and 41.8% unaccounted mass.

- 670 • Size-resolved BC mass concentration was measured on one occasion, with the mass sum of all
671 MOUDI stages reaching $14.3 \mu\text{g m}^{-3}$. Most of the BC mass (95%) was contained in the 0.1–1
672 μm range (i.e., the Greenfield gap) where wet scavenging by rain is [relatively](#) inefficient. The
673 measured BC peaked in the size range of 0.18 – 0.32 μm and accounted for 51.8% of the
674 measured PM for that stage. In the range of 0.10 – 0.18 μm , the mass percent contribution of
675 BC to the measured PM was 78.1%.
- 676 • Most of the total mass resided in the submicrometer mode (0.32–0.56 μm); however, one
677 MOUDI set revealed an additional supermicrometer mode (1.8–3.2 μm). Water-soluble
678 species that peaked in the submicrometer mode were associated with secondarily produced
679 species, including inorganic acids, amines, [Methanesulfonate \(MSA\)](#), and organic acids.
680 Water-soluble species that peaked in the supermicrometer mode were associated with sea salt
681 and crustal material. Most of the unaccounted mass was for $D_p > 0.32 \mu\text{m}$.
- 682 • The most abundant water-soluble species was SO_4^{2-} ($44\% \pm 6\%$), followed by NH_4^+ ($18\% \pm$
683 5%), NO_3^- ($10 \pm 3\%$), Na^+ ($8 \pm 3\%$), and Cl^- ($6\% \pm 3\%$). Correlation analysis revealed that
684 total water-soluble mass was most correlated with temperature ($r = 0.64$) and rainfall
685 accumulation ($r = -0.49$) among meteorological factors considered, although other factors were
686 likely influential such as wind direction and speed.
- 687 • Regardless of particle size, the majority of single particles examined with [energy dispersive](#)
688 [X-ray spectroscopy \(SEM-EDX\)](#) were non-spherical with evidence of agglomeration.
- 689 • PMF analysis suggested that there were five factors influencing the water-soluble fraction of
690 PM collected at the sampling site. These factors, their contribution to total water-soluble mass,
691 and the main species that permit them to be linked to a physical source are as follows: Aged
692 [Aerosol/Transported](#) (48.0%; NH_4^+ , SO_4^{2-} , MSA, oxalate), Sea Salt (22.5%; Cl^- , NO_3^- , Ca^{2+} ,
693 Na^+ , Mg^{2+} , Ba, Sr), Combustion (18.7%; Ni, As, Co, P, Mo, Cr), Vehicular/Resuspended Dust
694 (5.6%; Al, Ti, Fe), and Waste Processing (5.1%; Zn, Cd, Pb, Mn, Cu). The dominant
695 contribution of Aged/[Transported](#) aerosols to water-soluble mass contradicts two expectations:
696 (i) locally-produced sources in polluted cities should drown out the signal of transported
697 aerosols, and (ii) the signal of transported aerosols should be significantly reduced due to
698 scavenging processes upwind of the measurement site.

699

700 Although the current study focuses exclusively on the SWM season in Metro Manila,
701 results of this study are applicable to the study of aerosol impacts on Southeast Asia and other
702 regions. First, the [significant presence-detection](#) of Aged/~~Transported~~ aerosols [not only from local](#)
703 [but also from regional sources in Metro Manila indicates-confirms previous studies](#) that PM in the
704 region has the ability to travel long distances during the SWM season, ~~despite the typical~~
705 ~~assumption that wet scavenging effectively removes most of the particles~~. Characterization of
706 aerosols in Metro Manila is therefore important for better understanding the impacts that local
707 emissions will have on locations downwind of Metro Manila, including other populated cities in
708 Southeast and East Asia. Transport of pollution and decreased wet scavenging during the SWM
709 season may become increasingly important as studies have shown a decrease in SWM rainfall and
710 increase in the number of no-rain days during the SWM season in the western Philippines in recent
711 decades (e.g., Cruz et al., 2013).

712 Second, Southeast Asia has been named “one of the most hostile environments on the
713 planet for aerosol remote sensing” (Reid et al., 2013) [because of high cloud occurrence](#). Therefore,
714 space-based remote sensing of aerosol characteristics, such as retrievals of aerosol optical depth
715 (AOD), in this region are difficult. In situ measurements are critical for characterization of PM in
716 this region, especially during seasons such as the SWM when clouds are especially prevalent and
717 remote-sensing retrievals dependent on clear-sky conditions are lacking.

718 Third, this study provides a valuable dataset to compare to other regions impacted by
719 monsoons where the impacts of enhanced moisture and rainfall on size-resolved composition are
720 not well understood. As aqueous processing results in enhanced production of water-soluble
721 species (e.g., sulfate, organic acids), it is noteworthy for this monsoonal region that the water-
722 soluble fraction remains low relative to BC and other insoluble components. This has major
723 implications for the hygroscopicity of the regional PM.

724 Finally, the results of this study will be used to inform future sampling campaigns in this
725 region, including CAMP²Ex planned for the SWM season of 2019 based in the Philippines. As the
726 current MOUDI sampling campaign at [the Manila Observatory](#) is expected to extend for a full
727 year, future work will focus on changes in aerosol characteristics and sources on a seasonal basis.

728
729 *Data availability:* All data used in this work are available upon request.

730

731 *Author Contribution:* MTC, MOC, JBS, ABM, CS, and AS designed the experiments and all co-
732 authors carried out some aspect of the data collection. MTC, RAB, CS, LM, HD, and AS conducted
733 data analysis and interpretation. MTC and AS prepared the manuscript with contributions from all
734 co-authors.

735

736 *Competing interests:* The authors declare that they have no conflict of interest.

737

738 *Acknowledgements:* This research was funded by NASA grant 80NSSC18K0148. M. T. Cruz
739 acknowledges support from the Philippine Department of Science and Technology's ASTHRD
740 Program. R. A. Braun acknowledges support from the ARCS Foundation. A. B. MacDonald
741 acknowledges support from the Mexican National Council for Science and Technology
742 (CONACYT). We acknowledge Agilent Technologies for their support and Shane Snyder's
743 laboratories for ICP-QQQ data.

744

745 **References**

746 Adachi, K., and Tainosho, Y.: Characterization of heavy metal particles embedded in tire dust,
747 *Environ Int*, 30, 1009-1017, 10.1016/j.envint.2004.04.004, 2004.

748

749 Alas, H. D., Müller, T., Birmili, W., Kecorius, S., Cambaliza, M.O., Simpas, J. B., Cayetano, M.,
750 Weinhold, K., Vallar, E., Galvez, M.C., and Wiedensohler, A.: Spatial Characterization of Black
751 Carbon Mass Concentration in the Atmosphere of a Southeast Asian Megacity: An Air Quality
752 Case Study for Metro Manila, Philippines. *Aerosol Air Qual Res.*
753 doi.org/10.4209/aaqr.2017.08.0281, 2017.

754

755 Allen, H. C., Laux, J. M., Vogt, R., FinlaysonPitts, B. J., and Hemminger, J. C.: Water-induced
756 reorganization of ultrathin nitrate films on NaCl: Implications for the tropospheric chemistry of
757 sea salt particles, *J Phys Chem-US*, 100, 6371-6375, DOI 10.1021/jp953675a, 1996.

758

759 Allen, A. G., Nemitz, E., Shi, J. P., Harrison, R. M., and Greenwood, J. C.: Size distributions of
760 trace metals in atmospheric aerosols in the United Kingdom, *Atmos Environ*, 35, 4581-4591, Doi
761 10.1016/S1352-2310(01)00190-X, 2001.

762

763 Almeida, G. P., Bittencourt, A. T., Evangelista, M. S., Vieira-Filho, M. S., and Fornaro, A.:
764 Characterization of aerosol chemical composition from urban pollution in Brazil and its possible
765 impacts on the aerosol hygroscopicity and size distribution, *Atmos Environ*, 202, 149-159,
766 10.1016/j.atmosenv.2019.01.024, 2019.

767

768 Anderson, J. R., Aggett, F. J., Buseck, P. R., Germani, M. S., and Shattuck, T. W.: Chemistry of
769 Individual Aerosol-Particles from Chandler, Arizona, an Arid Urban-Environment, *Environ Sci*
770 *Technol*, 22, 811-818, DOI 10.1021/es00172a011, 1988.

771
772 Aswini, A. R., Hegde, P., Nair, P. R., and Aryasree, S.: Seasonal changes in carbonaceous
773 aerosols over a tropical coastal location in response to meteorological processes, *Science of The*
774 *Total Environment*, 656, 1261-1279, <https://doi.org/10.1016/j.scitotenv.2018.11.366>, 2019.
775
776 Bagtasa, G., Cayetano, M. G., and Yuan, C. S.: Seasonal variation and chemical characterization
777 of PM_{2.5} in northwestern Philippines, *Atmos Chem Phys*, 18, 4965-4980, 10.5194/acp-18-4965-
778 2018, 2018.
779
780 Bautista, A. T., Pabroa, P. C. B., Santos, F. L., Racho, J. M. D., and Quirrit, L. L.: Carbonaceous
781 particulate matter characterization in an urban and a rural site in the Philippines, *Atmos Pollut Res*,
782 5, 245-252, 10.5094/Apr.2014.030, 2014.
783
784 Begam, G. R., Vachaspati, C. V., Ahammed, Y. N., Kumar, K. R., Reddy, R. R., Sharma, S. K.,
785 Saxena, M., and Mandal, T. K.: Seasonal characteristics of water-soluble inorganic ions and
786 carbonaceous aerosols in total suspended particulate matter at a rural semi-arid site, Kadapa
787 (India), *Environmental Science and Pollution Research*, 24, 1719-1734, 10.1007/s11356-016-
788 7917-1, 2017.
789
790 Behera, S. N., Betha, R., Huang, X., and Balasubramanian, R.: Characterization and estimation of
791 human airway deposition of size-resolved particulate-bound trace elements during a recent haze
792 episode in Southeast Asia, *Environ Sci Pollut R*, 22, 4265-4280, 10.1007/s11356-014-3645-6,
793 2015.
794
795 Berresheim, H.: Biogenic Sulfur Emissions from the Sub-Antarctic and Antarctic Oceans, *J*
796 *Geophys Res-Atmos*, 92, 13245-13262, 10.1029/JD092iD11p13245, 1987.
797
798 Braun, R. A., Dadashazar, H., MacDonald, A. B., Aldhaif, A. M., Maudlin, L. C., Crosbie, E.,
799 Aghdam, M. A., Mardi, A. H., and Sorooshian, A.: Impact of Wildfire Emissions on Chloride
800 and Bromide Depletion in Marine Aerosol Particles, *Environ Sci Technol*, 51, 9013-9021,
801 10.1021/acs.est.7b02039, 2017.
802
803 Buchholz, B. A., and Landsberger, S.: Trace-Metal Analysis of Size-Fractionated Municipal Solid-
804 Waste Incinerator Fly-Ash and Its Leachates, *J Environ Sci Heal A*, 28, 423-441, Doi
805 10.1080/10934529309375887, 1993.
806
807 Burgermeister, S., and Georgii, H. W.: Distribution of Methanesulfonate, Nss Sulfate and
808 Dimethylsulfide over the Atlantic and the North-Sea, *Atmos Environ a-Gen*, 25, 587-595, Doi
809 10.1016/0960-1686(91)90056-D, 1991.
810
811 Chen, Y. Z., Shah, N., Huggins, F. E., and Huffman, G. P.: Microanalysis of ambient particles
812 from Lexington, KY, by electron microscopy, *Atmos Environ*, 40, 651-663,
813 10.1016/j.atmosenv.2005.09.036, 2006.
814

815 Chithra, V. S., and Nagendra, S. M. S.: Chemical and morphological characteristics of indoor and
816 outdoor particulate matter in an urban environment, *Atmos Environ*, 77, 579-587,
817 10.1016/j.atmosenv.2013.05.044, 2013.

818

819 Chuang, M.-T., Chang, S.-C., Lin, N.-H., Wang, J.-L., Sheu, G.-R., Chang, Y.-J., and Lee, C.-T.:
820 Aerosol chemical properties and related pollutants measured in Dongsha Island in the northern
821 South China Sea during 7-SEAS/Dongsha Experiment, *Atmospheric Environment*, 78, 82-92,
822 <https://doi.org/10.1016/j.atmosenv.2012.05.014>, 2013.

823

824 Clarke, A. D., Shinozuka, Y., Kapustin, V. N., Howell, S., Huebert, B., Doherty, S., Anderson,
825 T., Covert, D., Anderson, J., Hua, X., Moore, K. G., McNaughton, C., Carmichael, G., and
826 Weber, R.: Size distributions and mixtures of dust and black carbon aerosol in Asian outflow:
827 Physiochemistry and optical properties, *J Geophys Res-Atmos*, 109, Artn D15s09
828 10.1029/2003jd004378, 2004.

829

830 Coggon, M. M., Sorooshian, A., Wang, Z., Metcalf, A. R., Frossard, A. A., Lin, J. J., Craven, J.
831 S., Nenes, A., Jonsson, H. H., Russell, L. M., Flagan, R. C., and Seinfeld, J. H.: Ship impacts on
832 the marine atmosphere: insights into the contribution of shipping emissions to the properties of
833 marine aerosol and clouds, *Atmos Chem Phys*, 12, 8439-8458, 10.5194/acp-12-8439-2012, 2012.

834

835 Cohen, D. D., Stelcer, E., Santos, F. L., Prior, M., Thompson, C., and Pabroa, P. C. B.:
836 Fingerprinting and source apportionment of fine particle pollution in Manila by IBA and PMF
837 techniques: A 7-year study, *X-Ray Spectrom*, 38, 18-25, 10.1002/xrs.1112, 2009.

838

839 Crosbie, E., Sorooshian, A., Monfared, N. A., Shingler, T., and Esmaili, O.: A Multi-Year Aerosol
840 Characterization for the Greater Tehran Area Using Satellite, Surface, and Modeling Data,
841 *Atmosphere-Basel*, 5, 178-197, 10.3390/atmos5020178, 2014.

842

843 Crosbie, E., Youn, J. S., Balch, B., Wonaschutz, A., Shingler, T., Wang, Z., Conant, W. C.,
844 Betterton, E. A., and Sorooshian, A.: On the competition among aerosol number, size and
845 composition in predicting CCN variability: a multi-annual field study in an urbanized desert,
846 *Atmos Chem Phys*, 15, 6943-6958, 10.5194/acp-15-6943-2015, 2015.

847

848 Cruz, F. T., Narisma, G. T., Villafuerte, M. Q., Chua, K. U. C., and Olaguera, L. M.: A
849 climatological analysis of the southwest monsoon rainfall in the Philippines, *Atmos Res*, 122, 609-
850 616, 10.1016/j.atmosres.2012.06.010, 2013.

851

852 Csavina, J., Landazuri, A., Wonaschutz, A., Rine, K., Rheinheimer, P., Barbaris, B., Conant, W.,
853 Saez, A. E., and Betterton, E. A.: Metal and Metalloid Contaminants in Atmospheric Aerosols
854 from Mining Operations, *Water Air Soil Poll*, 221, 145-157, 10.1007/s11270-011-0777-x, 2011.

855

856 Dasgupta, P. K., Campbell, S. W., Al-Horr, R. S., Ullah, S. M. R., Li, J. Z., Amalfitano, C., and
857 Poor, N. D.: Conversion of sea salt aerosol to NaNO₃ and the production of HCl: Analysis of
858 temporal behavior of aerosol chloride/nitrate and gaseous HCl/HNO₃ concentrations with
859 AIM, *Atmos Environ*, 41, 4242-4257, 10.1016/j.atmosenv.2006.09.054, 2007.

860

861 Dumanoglu, Y., Kara, M., Altiok, H., Odabasi, M., Elbir, T., and Bayram, A.: Spatial and seasonal
862 variation and source apportionment of volatile organic compounds (VOCs) in a heavily
863 industrialized region, *Atmos Environ*, 98, 168-178, 10.1016/j.atmosenv.2014.08.048, 2014.
864

865 Ervens, B., Sorooshian, A., Aldhaif, A. M., Shingler, T., Crosbie, E., Ziemba, L., Campuzano-
866 Jost, P., Jimenez, J. L., and Wisthaler, A.: Is there an aerosol signature of chemical cloud
867 processing?, *Atmos Chem Phys*, 18, 16099-16119, 10.5194/acp-18-16099-2018, 2018.
868

869 Facchini, M. C., Decesari, S., Rinaldi, M., Carbone, C., Finessi, E., Mircea, M., Fuzzi, S.,
870 Moretti, F., Tagliavini, E., Ceburnis, D., and O'Dowd, C. D.: Important Source of Marine
871 Secondary Organic Aerosol from Biogenic Amines, *Environ Sci Technol*, 42, 9116-9121,
872 10.1021/es8018385, 2008.
873

874 Farren, N. J., Dunmore, R. E., Mead, M. I., Mohd Nadzir, M. S., Samah, A. A., Phang, S. M.,
875 Bandy, B. J., Sturges, W. T., and Hamilton, J. F.: Chemical characterisation of water-soluble
876 ions in atmospheric particulate matter on the east coast of Peninsular Malaysia, *Atmos. Chem.*
877 *Phys.*, 19, 1537-1553, 10.5194/acp-19-1537-2019, 2019.
878

879 Fitzgerald, J. W.: Marine Aerosols - a Review, *Atmos Environ a-Gen*, 25, 533-545, Doi
880 10.1016/0960-1686(91)90050-H, 1991.
881

882 Fraser, M. P., Cass, G. R., and Simoneit, B. R. T.: Air quality model evaluation data for organics.
883 6. C-3-C-24 organic acids, *Environ Sci Technol*, 37, 446-453, 10.1021/es0209262, 2003.
884

885 Fu, P. Q., Kawamura, K., Chen, J., Li, J., Sun, Y. L., Liu, Y., Tachibana, E., Aggarwal, S. G.,
886 Okuzawa, K., Tanimoto, H., Kanaya, Y., and Wang, Z. F.: Diurnal variations of organic
887 molecular tracers and stable carbon isotopic composition in atmospheric aerosols over Mt. Tai in
888 the North China Plain: an influence of biomass burning, *Atmos Chem Phys*, 12, 8359-8375,
889 10.5194/acp-12-8359-2012, 2012.
890

891 Fujimori, T., Takigami, H., Agusa, T., Eguchi, A., Bekki, K., Yoshida, A., Terazono, A., and
892 Ballesteros, F. C.: Impact of metals in surface matrices from formal and informal electronic-
893 waste recycling around Metro Manila, the Philippines, and intra-Asian comparison, *J Hazard*
894 *Mater*, 221-222, 139-146, <https://doi.org/10.1016/j.jhazmat.2012.04.019>, 2012.
895

896 Ge, X. L., Wexler, A. S., and Clegg, S. L.: Atmospheric amines - Part I. A review, *Atmos Environ*,
897 45, 524-546, 10.1016/j.atmosenv.2010.10.012, 2011.
898

899 Gietl, J. K., Lawrence, R., Thorpe, A. J., and Harrison, R. M.: Identification of brake wear particles
900 and derivation of a quantitative tracer for brake dust at a major road, *Atmos Environ*, 44, 141-146,
901 10.1016/j.atmosenv.2009.10.016, 2010.
902

903 Gullett, B. K., Linak, W. P., Touati, A., Wasson, S. J., Gatica, S., and King, C. J.: Characterization
904 of air emissions and residual ash from open burning of electronic wastes during simulated
905 rudimentary recycling operations, *J Mater Cycles Waste*, 9, 69-79, 10.1007/s10163-006-0161-x,
906 2007.
907

908 Harrison, R. M., Beddows, D. C. S., and Dall'Osto, M.: PMF Analysis of Wide-Range Particle
909 Size Spectra Collected on a Major Highway, *Environ Sci Technol*, 45, 5522-5528,
910 10.1021/es2006622, 2011.

911
912 Harrison, R. M., Jones, A. M., Gietl, J., Yin, J. X., and Green, D. C.: Estimation of the
913 Contributions of Brake Dust, Tire Wear, and Resuspension to Nonexhaust Traffic Particles
914 Derived from Atmospheric Measurements, *Environ Sci Technol*, 46, 6523-6529,
915 10.1021/es300894r, 2012.

916
917 Hitzenberger, R., and Tohno, S.: Comparison of black carbon (BC) aerosols in two urban areas –
918 concentrations and size distributions, *Atmospheric Environment*, 35, 2153-2167,
919 [https://doi.org/10.1016/S1352-2310\(00\)00480-5](https://doi.org/10.1016/S1352-2310(00)00480-5), 2001.

920
921 Hopke, P. K., Cohen, D. D., Begum, B. A., Biswas, S. K., Ni, B., Pandit, G. G., Santoso, M.,
922 Chung, Y. S., Davy, P., Markwitz, A., Waheed, S., Siddique, N., Santos, F. L., Pabroa, P. C. B.,
923 Seneviratne, M. C. S., Wimolwattanapun, W., Bunprapob, S., Vuong, T. B., Duy Hien, P. and
924 Markowicz, A.: Urban air quality in the Asian region, *Sci. Total Environ.*, 404(1), 103–112,
925 doi:10.1016/j.scitotenv.2008.05.039, 2008.

926
927 Huang, S. L., Rahn, K. A., and Arimoto, R.: Testing and optimizing two factor-analysis techniques
928 on aerosol at Narragansett, Rhode Island, *Atmos Environ*, 33, 2169-2185, Doi 10.1016/S1352-
929 2310(98)00324-0, 1999.

930
931 Iijima, A., Sato, K., Yano, K., Tago, H., Kato, M., Kimura, H., and Furuta, N.: Particle size and
932 composition distribution analysis of automotive brake abrasion dusts for the evaluation of
933 antimony sources of airborne particulate matter, *Atmos Environ*, 41, 4908-4919,
934 10.1016/j.atmosenv.2007.02.005, 2007.

935
936 Kahnert, M., Nousiainen, T., and Veihelmann, B.: Spherical and spheroidal model particles as an
937 error source in aerosol climate forcing and radiance computations: A case study for feldspar
938 aerosols, *J Geophys Res-Atmos*, 110, Artn D18s13, 10.1029/2004jd005558, 2005.

939
940 Kautzman, K. E., Surratt, J. D., Chan, M. N., Chan, A. W. H., Hersey, S. P., Chhabra, P. S.,
941 Dalleska, N. F., Wennberg, P. O., Flagan, R. C., and Seinfeld, J. H.: Chemical Composition of
942 Gas- and Aerosol-Phase Products from the Photooxidation of Naphthalene, *J Phys Chem A*, 114,
943 913-934, 10.1021/jp908530s, 2010.

944
945 Kawamura, K., and Ikushima, K.: Seasonal-Changes in the Distribution of Dicarboxylic-Acids in
946 the Urban Atmosphere, *Environ Sci Technol*, 27, 2227-2235, DOI 10.1021/es00047a033, 1993.

947
948 Kawamura, K., and Kaplan, I. R.: Motor Exhaust Emissions as a Primary Source for Dicarboxylic-
949 Acids in Los-Angeles Ambient Air, *Environ Sci Technol*, 21, 105-110, DOI
950 10.1021/es00155a014, 1987.

951
952 Kawamura, K., and Sakaguchi, F.: Molecular distributions of water soluble dicarboxylic acids in
953 marine aerosols over the Pacific Ocean including tropics, *J Geophys Res-Atmos*, 104, 3501-3509,
954 Doi 10.1029/1998jd100041, 1999.

955
956 Kecorius, S., Madueño, L., Löndahl, J., Vallar, E., Galvez, M. C., Idolor, L. F., Gonzaga-
957 Cayetano, M., Müller, T., Birmili, W., and Wiedensohler, A.: Respiratory tract deposition of
958 inhaled roadside ultrafine refractory particles in a polluted megacity of South-East Asia, *Science*
959 *of The Total Environment*, 663, 265-274, <https://doi.org/10.1016/j.scitotenv.2019.01.338>, 2019.
960
961 Kecorius, S., Madueno, L., Vallar, E., Alas, H., Betito, G., Birmili, W., Cambaliza, M. O., Catipay,
962 G., Gonzaga-Cayetano, M., Galvez, M. C., Lorenzo, G., Muller, T., Simpás, J. B., Tamayo, E. G.,
963 and Wiedensohler, A.: Aerosol particle mixing state, refractory particle number size distributions
964 and emission factors in a polluted urban environment: Case study of Metro Manila, Philippines,
965 *Atmos Environ*, 170, 169-183, [10.1016/j.atmosenv.2017.09.037](https://doi.org/10.1016/j.atmosenv.2017.09.037), 2017.
966
967 Keshtkar, H., and Ashbaugh, L. L.: Size distribution of polycyclic aromatic hydrocarbon
968 particulate emission factors from agricultural burning, *Atmos Environ*, 41, 2729-2739,
969 [10.1016/j.atmosenv.2006.11.043](https://doi.org/10.1016/j.atmosenv.2006.11.043), 2007.
970
971 Kim Oanh, N. T., Upadhyay, N., Zhuang, Y. H., Hao, Z. P., Murthy, D. V. S., Lestari, P., Villarin,
972 J. T., Chengchua, K., Co, H. X., Dung, N. T. and Lindgren, E. S.: Particulate air pollution in six
973 Asian cities: Spatial and temporal distributions, and associated sources, *Atmos. Environ.*, 40(18),
974 3367–3380, [doi:10.1016/j.atmosenv.2006.01.050](https://doi.org/10.1016/j.atmosenv.2006.01.050), 2006.
975
976 [Kim Oanh, N. T., Pongkiatkul, P., Cruz, M. T., Trung Dung, N., Phillip, L., Zhang, G., and Lestari,](#)
977 [P.: Monitoring and Source Apportionment for Particulate Matter Pollution in Six Asian Cities, in:](#)
978 [Integrated Air Quality Management: Asian Case Studies, Kim Oanh, N. T. \(Ed.\), CRC Press,](#)
979 [Taylor & Francis Group, USA, 97-124, 2013.](#)
980
981 Kleindienst, T. E., Jaoui, M., Lewandowski, M., Offenbergl, J. H., and Docherty, K. S.: The
982 formation of SOA and chemical tracer compounds from the photooxidation of naphthalene and its
983 methyl analogs in the presence and absence of nitrogen oxides, *Atmos Chem Phys*, 12, 8711-8726,
984 [10.5194/acp-12-8711-2012](https://doi.org/10.5194/acp-12-8711-2012), 2012.
985
986 Liao, H., Chen, W. T., and Seinfeld, J. H.: Role of climate change in global predictions of future
987 tropospheric ozone and aerosols, *J Geophys Res-Atmos*, 111, Artn D12304,
988 [10.1029/2005jd006852](https://doi.org/10.1029/2005jd006852), 2006.
989
990 Lin, C. C., Chen, S. J., Huang, K. L., Hwang, W. I., Chang-Chien, G. P., and Lin, W. Y.:
991 Characteristics of metals in nano/ultrafine/fine/coarse particles collected beside a heavily
992 trafficked road, *Environ Sci Technol*, 39, 8113-8122, [10.1021/es048182a](https://doi.org/10.1021/es048182a), 2005.
993
994 Linak, W. P., and Miller, C. A.: Comparison of particle size distributions and elemental
995 partitioning from the combustion of pulverized coal and residual fuel oil, *J Air Waste Manage*, 50,
996 1532-1544, [Doi 10.1080/10473289.2000.10464171](https://doi.org/10.1080/10473289.2000.10464171), 2000.
997
998 Ma, Y., Li, S., Zheng, J., Khalizov, A., Wang, X., Wang, Z., and Zhou, Y.: Size-resolved
999 measurements of mixing state and cloud-nucleating ability of aerosols in Nanjing, China, *Journal*
1000 *of Geophysical Research: Atmospheres*, 122, 9430-9450, [10.1002/2017jd026583](https://doi.org/10.1002/2017jd026583), 2017.
1001

1002 [Ma, L., Dadashazar, D., Braun, R. A., MacDonald, A. B., Aghdam, M. A., Maudlin, L. C., and](#)
1003 [Sorooshian, A.: Size-resolved characteristics of water-soluble particulate elements in a coastal](#)
1004 [area: Source identification, influence of wildfires, and diurnal variability, *Atmos. Environ.*, 206,](#)
1005 [72-84, <https://doi.org/10.1016/j.atmosenv.2019.02.045>, 2019.](#)
1006
1007 Mahowald, N., Jickells, T. D., Baker, A. R., Artaxo, P., Benitez-Nelson, C. R., Bergametti, G.,
1008 Bond, T. C., Chen, Y., Cohen, D. D., Herut, B., Kubilay, N., Losno, R., Luo, C., Maenhaut, W.,
1009 McGee, K. A., Okin, G. S., Siefert, R. L., and Tsukuda, S.: Global distribution of atmospheric
1010 phosphorus sources, concentrations and deposition rates, and anthropogenic impacts, *Global*
1011 *Biogeochem Cy*, 22, 10.1029/2008gb003240, 2008.
1012
1013 Marple, V., Olson, B., Romay, F., Hudak, G., Geerts, S. M. and Lundgren, D.: Second generation
1014 micro-orifice uniform deposit impactor, 120 MOUDI-II: Design, Evaluation, and application to
1015 long-term ambient sampling, *Aerosol Sci. Technol.*, 48(4), 427–433,
1016 doi:10.1080/02786826.2014.884274, 2014.
1017
1018 Martens, C. S., Wesolowski, J. J., Harriss, R. C., and Kaifer, R.: Chlorine Loss from Puerto-Rican
1019 and San-Francisco-Bay Area Marine Aerosols, *J Geophys Res*, 78, 8778-8792, DOI
1020 10.1029/JC078i036p08778, 1973.
1021
1022 Maudlin, L. C., Wang, Z., Jonsson, H. H., and Sorooshian, A.: Impact of wildfires on size-
1023 resolved aerosol composition at a coastal California site, *Atmos Environ*, 119, 59-68,
1024 10.1016/j.atmosenv.2015.08.039, 2015.
1025
1026 Metcalf, A. R., Craven, J. S., Ensberg, J. J., Brioude, J., Angevine, W., Sorooshian, A., Duong,
1027 H. T., Jonsson, H. H., Flagan, R. C., and Seinfeld, J. H.: Black carbon aerosol over the Los
1028 Angeles Basin during CalNex, *J Geophys Res-Atmos*, 117, 10.1029/2011jd017255, 2012.
1029
1030 Mielonen, T., Levy, R. C., Aaltonen, V., Komppula, M., de Leeuw, G., Huttunen, J., Lihavainen,
1031 H., Kolmonen, P., Lehtinen, K. E. J., and Arola, A.: Evaluating the assumptions of surface
1032 reflectance and aerosol type selection within the MODIS aerosol retrieval over land: the problem
1033 of dust type selection, *Atmos Meas Tech*, 4, 201-214, 10.5194/amt-4-201-2011, 2011.
1034
1035 Miller, J., and Miller, J.C.: *Statistics and chemometrics for analytical chemistry*. Pearson
1036 Education, 2018.
1037
1038 Mishra, S. K., Agnihotri, R., Yadav, P. K., Singh, S., Prasad, M. V. S. N., Praveen, P. S., Tawale,
1039 J. S., Rashmi, Mishra, N. D., Arya, B. C., and Sharma, C.: Morphology of Atmospheric Particles
1040 over Semi-Arid Region (Jaipur, Rajasthan) of India: Implications for Optical Properties, *Aerosol*
1041 *Air Qual Res*, 15, 974-+, 10.4209/aaqr.2014.10.0244, 2015.
1042
1043 Mooibroek, D., Schaap, M., Weijers, E. P., and Hoogerbrugge, R.: Source apportionment and
1044 spatial variability of PM_{2.5} using measurements at five sites in the Netherlands, *Atmospheric*
1045 *Environment*, 45, 4180-4191, 10.1016/j.atmosenv.2011.05.017, 2011.
1046
1047 Mosier, A. R., Andre, C. E., and Viets, F. G.: Identification of Aliphatic-Amines Volatilized from
1048 Cattle Feedyard, *Environ Sci Technol*, 7, 642-644, DOI 10.1021/es60079a009, 1973.

1049
1050 Muller, C., Iinuma, Y., Karstensen, J., van Pinxteren, D., Lehmann, S., Gnauk, T., and Herrmann,
1051 H.: Seasonal variation of aliphatic amines in marine sub-micrometer particles at the Cape Verde
1052 islands, *Atmos Chem Phys*, 9, 9587-9597, 2009.
1053
1054 Murphy, S. M., Agrawal, H., Sorooshian, A., Padro, L. T., Gates, H., Hersey, S., Welch, W. A.,
1055 Jung, H., Miller, J. W., Cocker, D. R., Nenes, A., Jonsson, H. H., Flagan, R. C., and Seinfeld, J.
1056 H.: Comprehensive Simultaneous Shipboard and Airborne Characterization of Exhaust from a
1057 Modern Container Ship at Sea, *Environ Sci Technol*, 43, 4626-4640, 10.1021/es802413j, 2009.
1058
1059 Norris, G., Duvall, R., Brown, S., and Bai, S.: EPA Positive Matrix Factorization (PMF) 5.0
1060 fundamentals and User Guide Prepared for the US Environmental Protection Agency Office of
1061 Research and Development, Washington, DC. Inc., Petaluma, 2014.
1062
1063 Nriagu, J. O.: A Global Assessment of Natural Sources of Atmospheric Trace-Metals, *Nature*, 338,
1064 47-49, DOI 10.1038/338047a0, 1989.
1065
1066 Pabroa, P. C. B., Santos, F. L., Morco, R. P., Racho, J. M. D., Bautista, A. T., and Bucal, C. G. D.:
1067 Receptor modeling studies for the characterization of air particulate lead pollution sources in
1068 Valenzuela sampling site (Philippines), *Atmos Pollut Res*, 2, 213-218, 10.5094/Apr.2011.027,
1069 2011.
1070
1071 Philippine Statistics Authority: <https://psa.gov.ph/>, Accessed 28 August 2018.
1072
1073 Polissar, A., Hopke, P., Paatero, P., Malm, W., and Sisler, J.: Atmospheric aerosol over Alaska 2.
1074 Elemental composition and sources. *Journal of Geophysical Research* 103, 19045-19057, 1998.
1075
1076 Prabhakar, G., Ervens, B., Wang, Z., Maudlin, L. C., Coggon, M. M., Jonsson, H. H., Seinfeld, J.
1077 H., and Sorooshian, A.: Sources of nitrate in stratocumulus cloud water: Airborne measurements
1078 during the 2011 E-PEACE and 2013 NiCE studies, *Atmos Environ*, 97, 166-173,
1079 10.1016/j.atmosenv.2014.08.019, 2014a.
1080
1081 Prabhakar, G., Sorooshian, A., Toffol, E., Arellano, A. F., and Betterton, E. A.: Spatiotemporal
1082 distribution of airborne particulate metals and metalloids in a populated arid region, *Atmos*
1083 *Environ*, 92, 339-347, 10.1016/j.atmosenv.2014.04.044, 2014b.
1084
1085 Qu, W. J., Wang, J., Zhang, X. Y., Wang, D., and Sheng, L. F.: Influence of relative humidity on
1086 aerosol composition: Impacts on light extinction and visibility impairment at two sites in coastal
1087 area of China, *Atmos Res*, 153, 500-511, 10.1016/j.atmosres.2014.10.009, 2015.
1088
1089 Raatikainen, T., Brus, D., Hyvärinen, A. P., Svensson, J., Asmi, E., and Lihavainen, H.: Black
1090 carbon concentrations and mixing state in the Finnish Arctic, *Atmos. Chem. Phys.*, 15, 10057-
1091 10070, 10.5194/acp-15-10057-2015, 2015.
1092
1093 Ramachandran, S., and Rajesh, T. A.: Black carbon aerosol mass concentrations over
1094 Ahmedabad, an urban location in western India: Comparison with urban sites in Asia, Europe,
1095 Canada, and the United States, *J Geophys Res-Atmos*, 112, 10.1029/2006jd007488, 2007.

1096
1097 Ran, L., Deng, Z. Z., Wang, P. C., and Xia, X. A.: Black carbon and wavelength-dependent aerosol
1098 absorption in the North China Plain based on two-year aethalometer measurements, *Atmos*
1099 *Environ*, 142, 132-144, 10.1016/j.atmosenv.2016.07.014, 2016.
1100
1101 Reddington, C. L., McMeeking, G., Mann, G. W., Coe, H., Frontoso, M. G., Liu, D., Flynn, M.,
1102 Spracklen, D. V., and Carslaw, K. S.: The mass and number size distributions of black carbon
1103 aerosol over Europe, *Atmos. Chem. Phys.*, 13, 4917-4939, 10.5194/acp-13-4917-2013, 2013.
1104
1105 Reff, A., Eberly, S.I., and Bhave, P.V.: Receptor modeling of ambient particulate matter data using
1106 positive matrix factorization: Review of existing methods. *J Air Waste Manage* 57, 146-154, 2007.
1107
1108 Reid, J. S., Xian, P., Hyer, E. J., Flatau, M. K., Ramirez, E. M., Turk, F. J., Sampson, C. R., Zhang,
1109 C., Fukada, E. M., and Maloney, E. D.: Multi-scale meteorological conceptual analysis of observed
1110 active fire hotspot activity and smoke optical depth in the Maritime Continent, *Atmos Chem Phys*,
1111 12, 2117-2147, 10.5194/acp-12-2117-2012, 2012.
1112
1113 Reid, J. S., Hyer, E. J., Johnson, R. S., Holben, B. N., Yokelson, R. J., Zhang, J. L., Campbell, J.
1114 R., Christopher, S. A., Di Girolamo, L., Giglio, L., Holz, R. E., Kearney, C., Miettinen, J., Reid,
1115 E. A., Turk, F. J., Wang, J., Xian, P., Zhao, G. Y., Balasubramanian, R., Chew, B. N., Janjai, S.,
1116 Lagrosas, N., Lestari, P., Lin, N. H., Mahmud, M., Nguyen, A. X., Norris, B., Oanh, N. T. K., Oo,
1117 M., Salinas, S. V., Welton, E. J., and Liew, S. C.: Observing and understanding the Southeast
1118 Asian aerosol system by remote sensing: An initial review and analysis for the Seven Southeast
1119 Asian Studies (7SEAS) program, *Atmos Res*, 122, 403-468, 10.1016/j.atmosres.2012.06.005,
1120 2013.
1121
1122 Reid, J. S., Xian, P., Holben, B. N., Hyer, E. J., Reid, E. A., Salinas, S. V., Zhang, J. L., Campbell,
1123 J. R., Chew, B. N., Holz, R. E., Kuciauskas, A. P., Lagrosas, N., Posselt, D. J., Sampson, C. R.,
1124 Walker, A. L., Welton, E. J., and Zhang, C. D.: Aerosol meteorology of the Maritime Continent
1125 for the 2012 7SEAS southwest monsoon intensive study - Part 1: regional-scale phenomena,
1126 *Atmos Chem Phys*, 16, 14041-14056, 10.5194/acp-16-14041-2016, 2016a.
1127
1128 Reid, J. S., Lagrosas, N. D., Jonsson, H. H., Reid, E. A., Atwood, S. A., Boyd, T. J., Ghate, V. P.,
1129 Xian, P., Posselt, D. J., Simpas, J. B., Uy, S. N., Zaiger, K., Blake, D. R., Bucholtz, A., Campbell,
1130 J. R., Chew, B. N., Cliff, S. S., Holben, B. N., Holz, R. E., Hyer, E. J., Kreidenweis, S. M.,
1131 Kuciauskas, A. P., Lolli, S., Oo, M., Perry, K. D., Salinas, S. V., Sessions, W. R., Smirnov, A.,
1132 Walker, A. L., Wang, Q., Yu, L. Y., Zhang, J. L., and Zhao, Y. J.: Aerosol meteorology of
1133 Maritime Continent for the 2012 7SEAS southwest monsoon intensive study - Part 2: Philippine
1134 receptor observations of fine-scale aerosol behavior, *Atmos Chem Phys*, 16, 14057-14078,
1135 10.5194/acp-16-14057-2016, 2016b.
1136
1137 Rocha, L. D. S., and Correa, S. M.: Determination of size-segregated elements in diesel-biodiesel
1138 blend exhaust emissions, *Environ Sci Pollut R*, 25, 18121-18129, 10.1007/s11356-018-1980-8,
1139 2018.
1140

1141 Rogge, W. F., Mazurek, M. A., Hildemann, L. M., Cass, G. R., and Simoneit, B. R. T.:
1142 Quantification of Urban Organic Aerosols at a Molecular-Level - Identification, Abundance and
1143 Seasonal-Variation, *Atmos Environ a-Gen*, 27, 1309-1330, Doi 10.1016/0960-1686(93)90257-Y,
1144 1993.

1145

1146 Ro, C. U., Oh, K. Y., Kim, H., Kim, Y. P., Lee, C. B., Kim, K. H., Kang, C. H., Osan, J., De
1147 Hoog, J., Worobiec, A., and Van Grieken, R.: Single-particle analysis of aerosols at Cheju
1148 Island, Korea, using low-Z electron probe X-ray microanalysis: A direct proof of nitrate
1149 formation from sea salts, *Environ Sci Technol*, 35, 4487-4494, 10.1021/es0155231, 2001.

1150

1151 Rolph, G.D.: Real-time Environmental Applications and Display sYstem (READY) website
1152 (<http://ready.Arl.NOAA.Gov>), NOAA Air Resour. Lab., Silver Spring, Md., 2016.

1153

1154 Roth, B., and Okada, K.: On the modification of sea-salt particles in the coastal atmosphere,
1155 *Atmos Environ*, 32, 1555-1569, Doi 10.1016/S1352-2310(97)00378-6, 1998.

1156

1157 Saltzman, E. S., Savoie, D. L., Zika, R. G., and Prospero, J. M.: Methane Sulfonic-Acid in the
1158 Marine Atmosphere, *J Geophys Res-Oceans*, 88, 897-902, DOI 10.1029/JC088iC15p10897, 1983.

1159

1160 Saltzman, E. S., Savoie, D. L., Prospero, J. M., and Zika, R. G.: Methanesulfonic-Acid and Non-
1161 Sea-Salt Sulfate in Pacific Air - Regional and Seasonal-Variations, *J Atmos Chem*, 4, 227-240,
1162 Doi 10.1007/Bf00052002, 1986.

1163

1164 Schade, G. W., and Crutzen, P. J.: Emission of Aliphatic-Amines from Animal Husbandry and
1165 Their Reactions - Potential Source of N₂O and HCN, *J Atmos Chem*, 22, 319-346, Doi
1166 10.1007/Bf00696641, 1995.

1167

1168 [Schlosser, J. S., Braun, R. A., Bradley, T., Dadashazar, H., MacDonald, A. B., Aldhaif, A. M.,](#)
1169 [Aghdam, M. A., Mardi, A. H., Xian, P., and Sorooshian, A.: Analysis of Aerosol Composition](#)
1170 [Data for Western United States Wildfires Between 2005-2015: Dust Emissions, Chloride](#)
1171 [Depletion, and Most Enhanced Aerosol Constituents, *J. Geophys. Res.*, 122,](#)
1172 [doi:10.1002/2017JD026547, 2017.](https://doi.org/10.1002/2017JD026547)

1173

1174 Schwarz, J. P., Gao, R. S., Spackman, J. R., Watts, L. A., Thomson, D. S., Fahey, D. W., Ryerson,
1175 T. B., Peischl, J., Holloway, J. S., Trainer, M., Frost, G. J., Baynard, T., Lack, D. A., de Gouw, J.
1176 A., Warneke, C., and Del Negro, L. A.: Measurement of the mixing state, mass, and optical size
1177 of individual black carbon particles in urban and biomass burning emissions, *Geophysical*
1178 *Research Letters*, 35, 10.1029/2008gl033968, 2008.

1179

1180 Seinfeld, J. H., and Pandis, S. N.: Atmospheric chemistry and physics (3rd ed.). New York: Wiley-
1181 Interscience, 2016.

1182

1183 Shafer, M. M., Toner, B. M., Oyerdier, J. T., Schauer, J. J., Fakra, S. C., Hu, S. H., Herner, J. D.,
1184 and Ayala, A.: Chemical Speciation of Vanadium in Particulate Matter Emitted from Diesel
1185 Vehicles and Urban Atmospheric Aerosols, *Environ Sci Technol*, 46, 189-195,
1186 10.1021/es200463c, 2012.

1187
1188 Shingler, T., Sorooshian, A., Ortega, A., Crosbie, E., Wonaschutz, A., Perring, A. E.,
1189 Beyersdorf, A., Ziemba, L., Jimenez, J. L., Campuzano-Jost, P., Mikoviny, T., Wisthaler, A., and
1190 Russell, L. M.: Ambient observations of hygroscopic growth factor and $f(\text{RH})$ below 1: Case
1191 studies from surface and airborne measurements, *J Geophys Res-Atmos*, 121, 13661-13677,
1192 10.1002/2016jd025471, 2016.
1193
1194 Shiraiwa, M., Kondo, Y., Moteki, N., Takegawa, N., Sahu, L. K., Takami, A., Hatakeyama, S.,
1195 Yonemura, S., and Blake, D. R.: Radiative impact of mixing state of black carbon aerosol in Asian
1196 outflow, *Journal of Geophysical Research: Atmospheres*, 113, 10.1029/2008jd010546, 2008.
1197
1198 Simpas, J., Lorenzo, G., and Cruz, M. T.: Monitoring Particulate Matter Levels and Composition
1199 for Source Apportionment Study in Metro Manila, Philippines, in: *Improving Air Quality in Asian*
1200 *Developing Countries: Compilation of Research Findings*, Kim Oanh, N. T. (Ed.), NARENCA,
1201 Vietnam Publishing House of Natural Resources, Environment and Cartography, Vietnam, 239-
1202 261, 2014.
1203
1204 Singh, M., Jaques, P. A., and Sioutas, C.: Size distribution and diurnal characteristics of particle-
1205 bound metals in source and receptor sites of the Los Angeles Basin, *Atmos Environ*, 36, 1675-
1206 1689, Pii S1352-2310(02)00166-8, Doi 10.1016/S1352-2310(02)00166-8, 2002.
1207
1208 Song, F., and Gao, Y.: Size distributions of trace elements associated with ambient particular
1209 matter in the affinity of a major highway in the New Jersey-New York metropolitan area, *Atmos*
1210 *Environ*, 45, 6714-6723, 10.1016/j.atmosenv.2011.08.031, 2011.
1211
1212 Sorooshian, A., Ng, N. L., Chan, A. W. H., Feingold, G., Flagan, R. C., and Seinfeld, J. H.:
1213 Particulate organic acids and overall water-soluble aerosol composition measurements from the
1214 2006 Gulf of Mexico Atmospheric Composition and Climate Study (GoMACCS), *J Geophys*
1215 *Res-Atmos*, 112, 10.1029/2007jd008537, 2007.
1216
1217 Sorooshian, A., Murphy, S. N., Hersey, S., Gates, H., Padro, L. T., Nenes, A., Brechtel, F. J.,
1218 Jonsson, H., Flagan, R. C., and Seinfeld, J. H.: Comprehensive airborne characterization of aerosol
1219 from a major bovine source, *Atmos Chem Phys*, 8, 5489-5520, DOI 10.5194/acp-8-5489-2008,
1220 2008.
1221
1222 Sorooshian, A., Padro, L. T., Nenes, A., Feingold, G., McComiskey, A., Hersey, S. P., Gates, H.,
1223 Jonsson, H. H., Miller, S. D., Stephens, G. L., Flagan, R. C., and Seinfeld, J. H.: On the link
1224 between ocean biota emissions, aerosol, and maritime clouds: Airborne, ground, and satellite
1225 measurements off the coast of California, *Global Biogeochem Cy*, 23,
1226 10.1029/2009gb003464, 2009.
1227
1228 Sorooshian, A., Crosbie, E., Maudlin, L. C., Youn, J. S., Wang, Z., Shingler, T., Ortega, A. M.,
1229 Hersey, S., and Woods, R. K.: Surface and airborne measurements of organosulfur and
1230 methanesulfonate over the western United States and coastal areas, *J Geophys Res-Atmos*, 120,
1231 8535-8548, 10.1002/2015jd023822, 2015.
1232

1233 Stein, A. F., Draxler, R. R., Rolph, G. D., Stunder, B. J. B., Cohen, M. D., and Ngan, F.: NOAA's
1234 Hysplit Atmospheric Transport and Dispersion Modeling System, *B Am Meteorol Soc*, 96, 2059-
1235 2077, 10.1175/Bams-D-14-00110.1, 2015.

1236
1237 Tai, A. P. K., Mickley, L. J., and Jacob, D. J.: Correlations between fine particulate matter (PM_{2.5})
1238 and meteorological variables in the United States: Implications for the sensitivity of PM_{2.5} to
1239 climate change, *Atmos Environ*, 44, 3976-3984, 10.1016/j.atmosenv.2010.06.060, 2010.

1240
1241 Tsakalou, C., Papamarkou, S., Tsakiridis, P. E., Bartzas, G., and Tsakalakis, K.: Characterization
1242 and leachability evaluation of medical wastes incineration fly and bottom ashes and their
1243 vitrification outgrowths, *J Environ Chem Eng*, 6, 367-376, 10.1016/j.jece.2017.12.012, 2018.

1244
1245 [U.S. Environmental Protection Agency: Monitoring PM_{2.5} in Ambient Air](#)
1246 [Using Designated Reference or Class I Equivalent Methods. Report No. EPA-454/B-16-001. US](#)
1247 [Environmental Protection Agency, Research Triangle Park, NC., 2016.](#)

1248
1249 VandenBoer, T. C., Petroff, A., Markovic, M. Z., and Murphy, J. G.: Size distribution of alkyl
1250 amines in continental particulate matter and their online detection in the gas and particle phase,
1251 *Atmos Chem Phys*, 11, 4319-4332, 10.5194/acp-11-4319-2011, 2011.

1252
1253 Villafuerte, M. Q., Matsumoto, J., Akasaka, I., Takahashi, H. G., Kubota, H., and Cinco, T. A.:
1254 Long-term trends and variability of rainfall extremes in the Philippines, *Atmos Res*, 137, 1-13,
1255 10.1016/j.atmosres.2013.09.021, 2014.

1256
1257 Vossler, T., Cernikovskiy, L., Novak, J., and Williams, R.: Source apportionment with
1258 uncertainty estimates of fine particulate matter in Ostrava, Czech Republic using Positive Matrix
1259 Factorization, *Atmos Pollut Res*, 7, 503-512, 10.1016/j.apr.2015.12.004, 2016.

1260
1261 Wang, J., Ge, C., Yang, Z. F., Hyer, E. J., Reid, J. S., Chew, B. N., Mahmud, M., Zhang, Y. X.,
1262 and Zhang, M. G.: Mesoscale modeling of smoke transport over the Southeast Asian Maritime
1263 Continent: Interplay of sea breeze, trade wind, typhoon, and topography, *Atmos Res*, 122, 486-
1264 503, 10.1016/j.atmosres.2012.05.009, 2013.

1265
1266 Wang, Y. Q., Zhang, X. Y., and Draxler, R. R.: TrajStat: GIS-based software that uses various
1267 trajectory statistical analysis methods to identify potential sources from long-term air pollution
1268 measurement data, *Environ Modell Softw*, 24, 938-939, 10.1016/j.envsoft.2009.01.004, 2009.

1269
1270 Wasson, S. J., Linak, W. P., Gullett, B. K., King, C. J., Touati, A., Huggins, F. E., Chen, Y. Z.,
1271 Shah, N., and Huffman, G. P.: Emissions of chromium, copper, arsenic, and PCDDs/Fs from open
1272 burning of CCA-treated wood, *Environ Sci Technol*, 39, 8865-8876, 10.1021/es050891g, 2005.

1273
1274 Watson, J. G.: Protocol for Applying and Validating the CMB Model for PM_{2.5} and VOC. Report
1275 No. EPA-451/R-04-001. US Environmental Protection Agency, Research Triangle Park, NC.,
1276 2004.

1277

1278 Watts, S. F., Watson, A., and Brimblecombe, P.: Measurements of the Aerosol Concentrations of
1279 Methanesulfonic Acid, Dimethyl-Sulfoxide and Dimethyl Sulfone in the Marine Atmosphere of
1280 the British-Isles, *Atmos Environ*, 21, 2667-2672, Doi 10.1016/0004-6981(87)90198-3, 1987.
1281
1282 Wonaschuetz, A., Sorooshian, A., Ervens, B., Chuang, P. Y., Feingold, G., Murphy, S. M., de
1283 Gouw, J., Warneke, C., and Jonsson, H. H.: Aerosol and gas re-distribution by shallow cumulus
1284 clouds: An investigation using airborne measurements, *J Geophys Res-Atmos*, 117,
1285 10.1029/2012jd018089, 2012.
1286
1287 Wu, D., Zhang, F., Lou, W. H., Li, D., and Chen, J. M.: Chemical characterization and toxicity
1288 assessment of fine particulate matters emitted from the combustion of petrol and diesel fuels, *Sci*
1289 *Total Environ*, 605, 172-179, 10.1016/j.scitotenv.2017.06.058, 2017.
1290
1291 Xian, P., Reid, J. S., Atwood, S. A., Johnson, R. S., Hyer, E. J., Westphal, D. L., and Sessions, W.:
1292 Smoke aerosol transport patterns over the Maritime Continent, *Atmos Res*, 122, 469-485,
1293 10.1016/j.atmosres.2012.05.006, 2013.
1294
1295 Xu, G. J., and Gao, Y.: Characterization of marine aerosols and precipitation through shipboard
1296 observations on the transect between 31 degrees N-32 degrees S in the West Pacific, *Atmos Pollut*
1297 *Res*, 6, 154-161, 10.5094/Apr.2015.018, 2015.
1298
1299 Yao, X. H., Fang, M., and Chan, C. K.: The size dependence of chloride depletion in fine and
1300 coarse sea-salt particles, *Atmos Environ*, 37, 743-751, 10.1016/S1352-2310(02)00955-X, 2003.
1301
1302 Youn, J. S., Wang, Z., Wonaschutz, A., Arellano, A., Betterton, E. A., and Sorooshian, A.:
1303 Evidence of aqueous secondary organic aerosol formation from biogenic emissions in the North
1304 American Sonoran Desert, *Geophys Res Lett*, 40, 3468-3472, 10.1002/grl.50644, 2013.
1305
1306 Youn, J. S., Crosbie, E., Maudlin, L. C., Wang, Z., and Sorooshian, A.: Dimethylamine as a major
1307 alkyl amine species in particles and cloud water: Observations in semi-arid and coastal regions,
1308 *Atmos Environ*, 122, 250-258, 10.1016/j.atmosenv.2015.09.061, 2015.
1309
1310 Youn, J. S., Csavina, J., Rine, K. P., Shingler, T., Taylor, M. P., Saez, A. E., Betterton, E. A., and
1311 Sorooshian, A.: Hygroscopic Properties and Respiratory System Deposition Behavior of
1312 Particulate Matter Emitted By Mining and Smelting Operations, *Environ Sci Technol*, 50, 11706-
1313 11713, 10.1021/acs.est.6b03621, 2016.
1314

1315 **Table 1.** Summary of average operating parameters, meteorological conditions, and total resolved
 1316 water-soluble mass concentration for each MOUDI sample set collected at Manila Observatory
 1317 (MO) during the 2018 Southwest Monsoon period. On two occasions, simultaneous MOUDI sets
 1318 were collected for one set to undergo gravimetric analysis (MO3 and MO13) to compare with mass
 1319 resolved from chemical speciation of the water-soluble fraction (MO4 and MO14). One additional
 1320 MOUDI set devoted to microscopy analysis was collected using aluminum substrates for one hour
 1321 on August 1 at 30 LPM.
 1322

Sample set name	Dates	Durati on (hrs)	Flow rate (LPM)	Wind speed (m/s)	Wind direction (°)	T (°C)	Rain (mm)	Water-soluble mass ($\mu\text{g m}^{-3}$)
MO1	Jul 19-20	24	30	3.3	90.1	24.9	47	4.6
MO2	Jul 23-25	54	30	1.3	95.8	26.7	7.8	6.5
MO3/4	Jul 25-30	119	28/30	1.2	111.8	26.7	49.6	5.2
MO5	Jul 30-Aug 1	42	29	2.6	98.1	27.5	52.8	9.2
MO6	Aug 6-8	48	27	0.9	127.5	26.1	30.4	5.1
MO7	Aug 14-16	48	28	3.0	107.8	27.8	2.8	13.7
MO8	Aug 22-24	48	29	3.5	108.7	28.1	1	12.8
MO9	Sep 1-3	48	27	0.7	98.6	26.6	51.6	6.2
MO10	Sep 10–12	48	29	1.0	94.7	26.2	78.4	6.4
MO11	Sep 18–20	48	27	0.5	290.2	27.8	0	2.7
MO12	Sep 26-28	48	27	1.2	96.3	27.8	6.8	13.5
MO13/14	Oct 6-8	48	28/26	0.6	108.2	27.8	0.8	16.6

1323
 1324

1325 **Table 2.** Charge balance slopes (cations on y-axis; anions on x-axis) for the MOUDI sets shown
 1326 including the averages of all sets (All) for three size ranges: submicrometer stages spanning 0.056
 1327 – 1.0 μm ; supermicrometer stages ($> 1.0 \mu\text{m}$); and all stages ($> 0.056 \mu\text{m}$). The species used in
 1328 the charge balance analysis include those speciated with the IC (listed in Section 2.3) plus K from
 1329 ICP-QQQ analysis.
 1330

Sample set	0.056 – 1.0 μm	$> 1 \mu\text{m}$	$> 0.056 \mu\text{m}$
MO1	0.87	1.37	0.89
MO2	1.46	1.26	1.41
MO4	1.25	1.17	1.21
MO5	1.35	1.43	1.41
MO6	1.29	1.45	1.31
MO7	1.40	1.23	1.36
MO8	1.35	1.33	1.36
MO9	1.28	1.55	1.26
MO10	1.37	1.36	1.35
MO11	0.97	1.60	1.27
MO12	1.37	1.19	1.33
MO14	1.31	1.28	1.29
All	1.35	1.24	1.33

1331
 1332

1333 **Table 3.** Contributions (in weight percentage) of each PMF source factor to the total mass in
 1334 different diameter ranges.
 1335

Diameter Range (μm)	Aged/ Transported	Sea Salt	Combustion	Vehicular/ Resuspended Dust	Waste Processing
> 0.056	48.0%	22.5%	18.7%	5.6%	5.1%
0.056 - 1.0	68.9%	0.6%	23.9%	1.5%	5.1%
> 1.0	18.6%	53.5%	11.3%	11.3%	5.3%

1336

1337 **Table 4.** Correlation matrix (r values) between water-soluble species based on total MOUDI-
 1338 integrated mass concentrations (> 0.056 μm). Blank cells represent statistically insignificant
 1339 values. Results for the sub- and supermicrometer ranges are in Tables S2-S3. Panels A-E
 1340 represent important species from each of the source profiles identified in Section 3.3: A =
 1341 Aged/Transported, B = Sea Salt, C = Combustion, D = Vehicular/Resuspended Dust, E = Waste
 1342 Processing. DMA – Dimethylamine, MSA – Methanesulfonate, PH – Phthalate, OX – Oxalate,
 1343 MA – Maleate, SU – Succinate, AD – Adipate.
 1344

A)															
OX	1.00														
SO₄	0.74	1.00													
NH₄	0.68	0.99	1.00												
Sn	0.71	0.87	0.85	1.00											
Rb	0.73	0.74	0.73	0.69	1.00										
K	0.76	0.71	0.69	0.69	0.97	1.00									
Cs	0.72	0.82	0.81	0.74	0.96	0.91	1.00								
V	0.36	0.64	0.63	0.48	0.53	0.51	0.57	1.00							
DMA		0.35		0.38	0.45	0.37	0.45		1.00						
MSA	0.71	0.89	0.89	0.79	0.90	0.85	0.92	0.51	0.47	1.00					
PH	0.68	0.67	0.68	0.73	0.82	0.76	0.80		0.38	0.88	1.00				
SU	0.63	0.56	0.59	0.44	0.87	0.81	0.82		0.68	0.78	0.84	1.00			
AD	0.40	0.66	0.70	0.62	0.70	0.70	0.77		0.84	0.74	0.75	0.90	1.00		
Se	0.75	0.75	0.73	0.66	0.80	0.78	0.79	0.32	0.34	0.78	0.80	0.88	0.88	1.00	
Tl	0.75	0.87	0.86	0.80	0.89	0.85	0.94	0.74	0.65	0.80	0.52	0.70		0.43	1.00
	OX	SO₄	NH₄	Sn	Rb	K	Cs	V	DMA	MSA	PH	SU	AD	Se	Tl

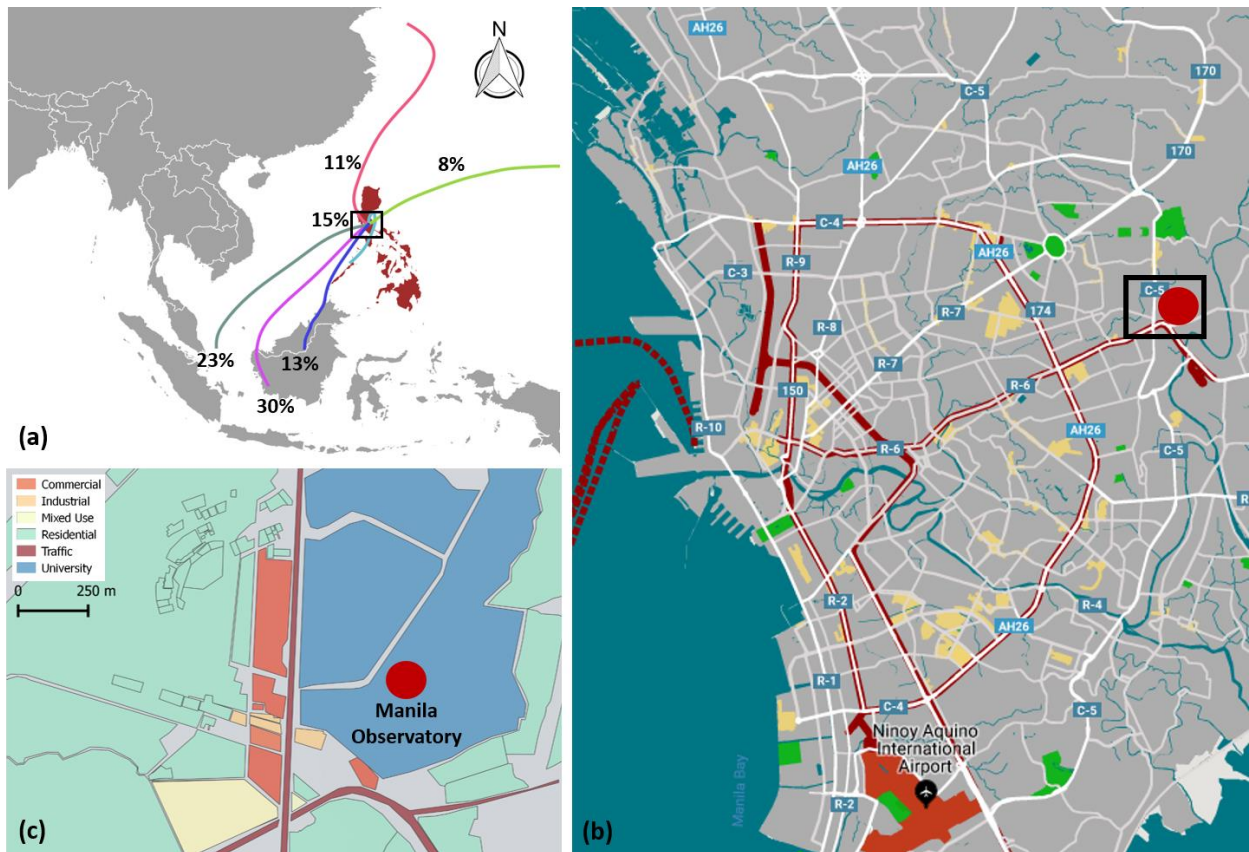
B)								
Cl	1.00							
NO₃	0.76	1.00						
Ba	0.66	0.80	1.00					
Sr	0.78	0.87	0.91	1.00				
Ca	0.58	0.79	0.75	0.78	1.00			
Na	0.93	0.87	0.75	0.85	0.63	1.00		
Mg	0.91	0.87	0.77	0.87	0.66	0.99	1.00	
Hf					0.57			1.00
	Cl	NO₃	Ba	Sr	Ca	Na	Mg	Hf

C)							
As	1.00						
Ni	0.58	1.00					
Co			1.00				
P		0.33	0.34	1.00			
Mo					1.00		
Cr	0.62	0.49		0.20		1.00	
MA			0.67		-0.42		1.00
Ag			0.85		0.64		1.00
	As	Ni	Co	P	Mo	Cr	Mal

D)						
Zr	1.00					
Y	0.75	1.00				
Al	0.88	0.76	1.00			
Fe	0.33	0.61	0.25	1.00		
Ti	0.84	0.66	0.82	0.41	1.00	
Nb	0.70	0.50	0.59	0.59	0.70	1.00
	Zr	Y	Al	Fe	Ti	Nb

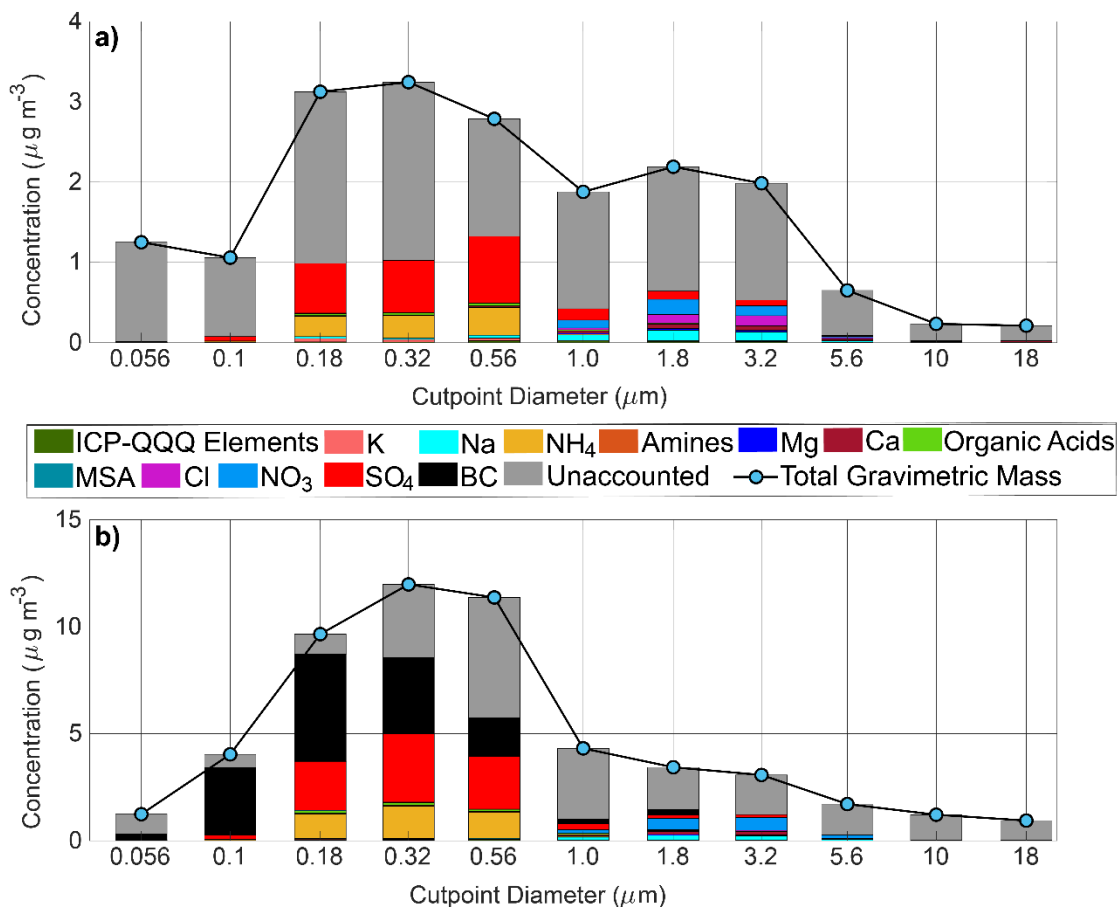
E)					
Cd	1.00				
Zn	0.60	1.00			
Cu	0.21	0.27	1.00		
Mn	0.28	0.61	0.22	1.00	
Pb	0.78	0.58	0.38	0.27	1.00
	Cd	Zn	Cu	Mn	Pb

1345
 1346
 1347
 1348



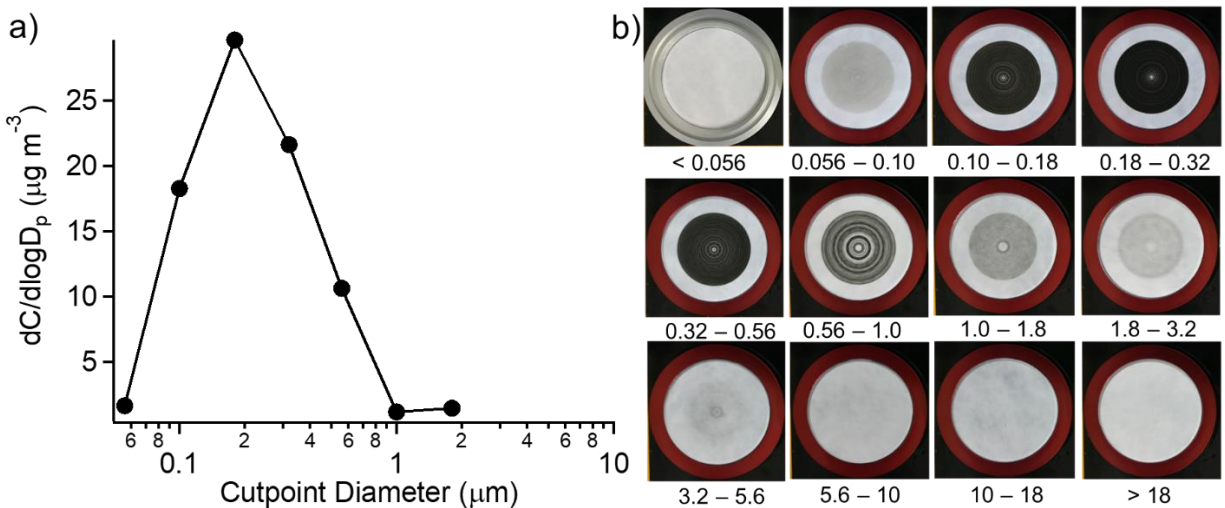
1349
 1350 **Figure 1.** (a) Location of Metro Manila, Philippines relative to Southeast Asia. Also shown are
 1351 5-day backward trajectory frequencies during the sampling duration based on HYSPLIT cluster
 1352 analysis; note that 15% correspond to trajectories within the black square. (b) Close-up view of
 1353 Metro Manila showing the location of the Manila Observatory sampling site with a black rectangle.
 1354 The base map shows roads, commercial centers, and major transit lines in the city. (c) Land use
 1355 classification in the vicinity of the sampling site. (Sources: GADM, Snazzy Maps, OpenStreetMap,
 1356 NOAA HYSPLIT, & TrajSat)

1357
 1358
 1359
 1360
 1361
 1362



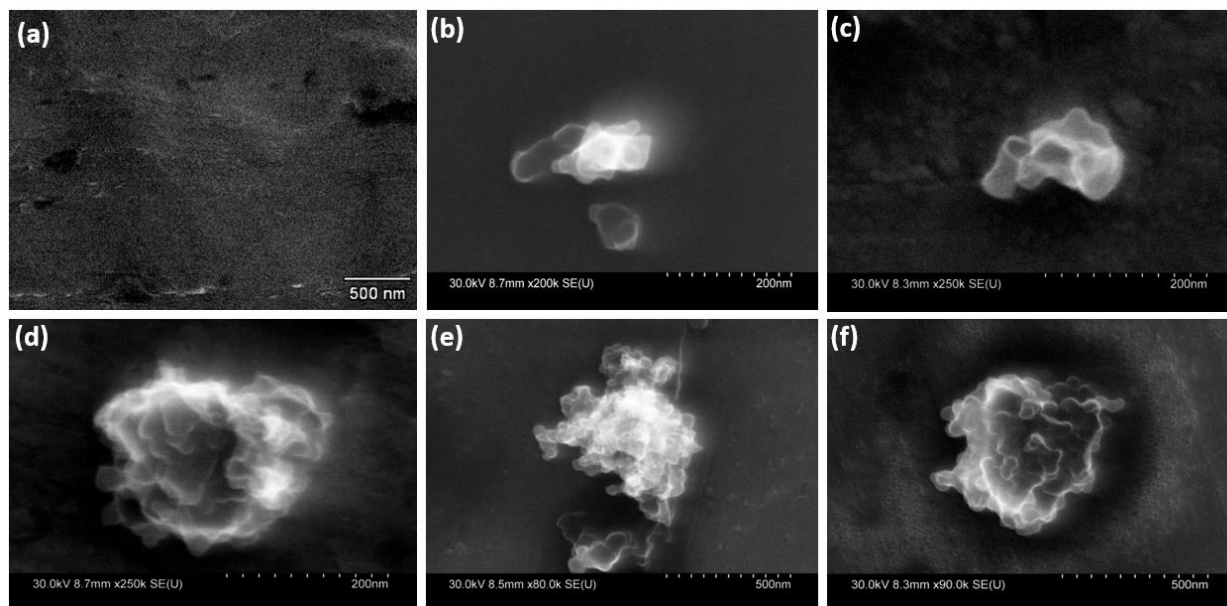
1363
 1364 **Figure 2.** Mass size distributions of total PM (blue markers) and resolved chemical species
 1365 (colored bars) for MOUDI sets (a) MO3/4 and (b) MO13/14. Note that set MO13 was the single
 1366 MOUDI set where BC was quantified. ICP-QQQ = sum of water-soluble elements except K;
 1367 amines = sum of DMA, TMA, DEA; organic acids = sum of oxalate, succinate, adipate,
 1368 pyruvate, phthalate, maleate.
 1369

1370



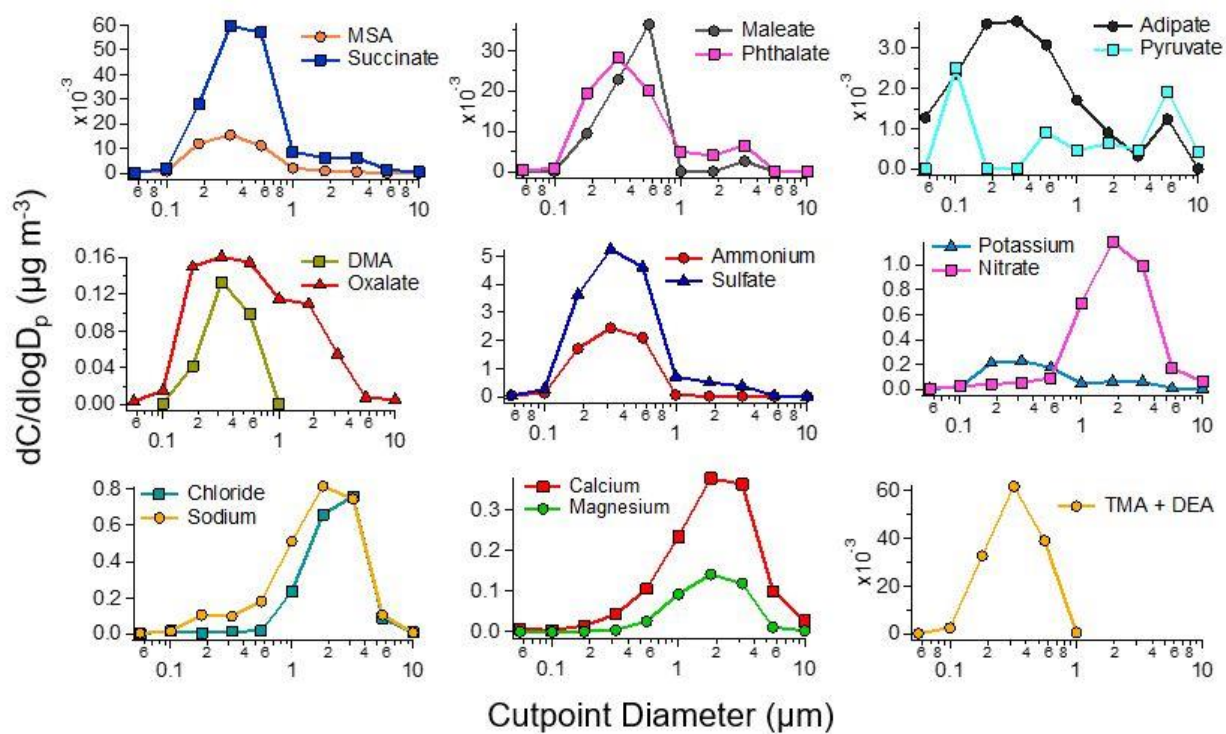
1371
1372
1373
1374
1375
1376

Figure 3. (a) Mass size distribution of BC retrieved from the MABI optical measurement at 870 nm for set MO13. Missing values were below detection limits. (b) Photographs of each stage of set MO13 with numbers below each image representing the aerodynamic diameter ranges in units of μm .



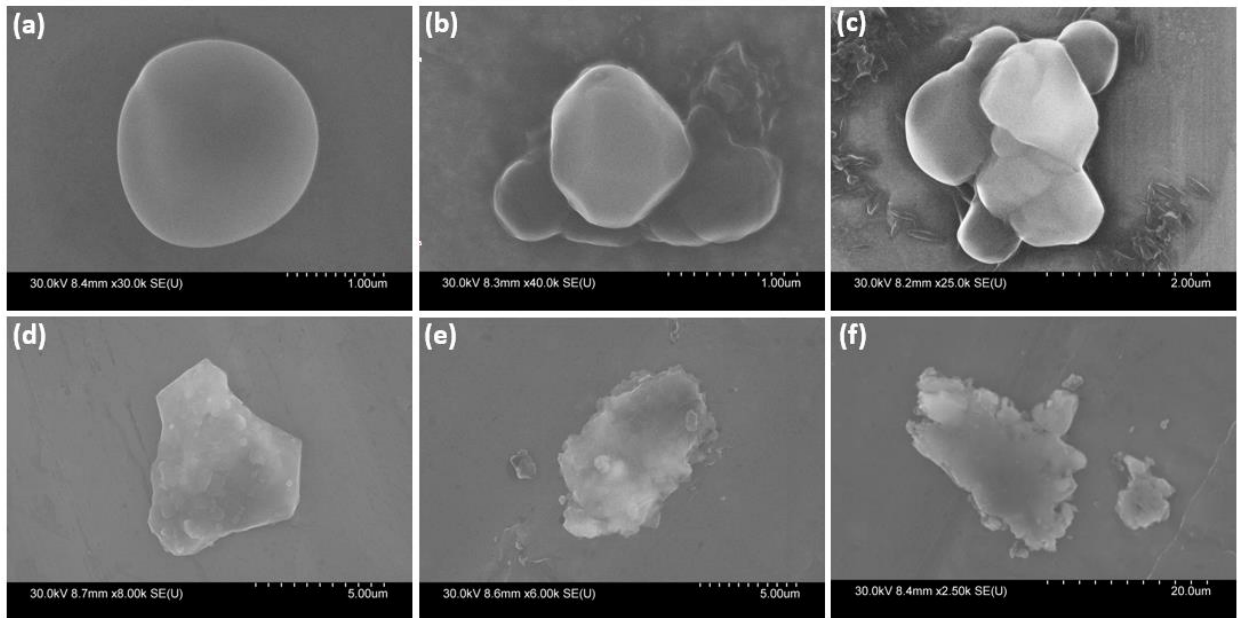
1377
1378
1379
1380
1381

Figure 4. SEM image of a (a) blank filter and (b-f) individual particles in different sub-micrometer aerodynamic diameter ranges sampled by the MOUDI: (b) 0.056–0.1 μm , (c) 0.1–0.18 μm , (d) 0.18–0.32 μm , (e) 0.32–0.56 μm , (f) 0.56–1.0 μm .



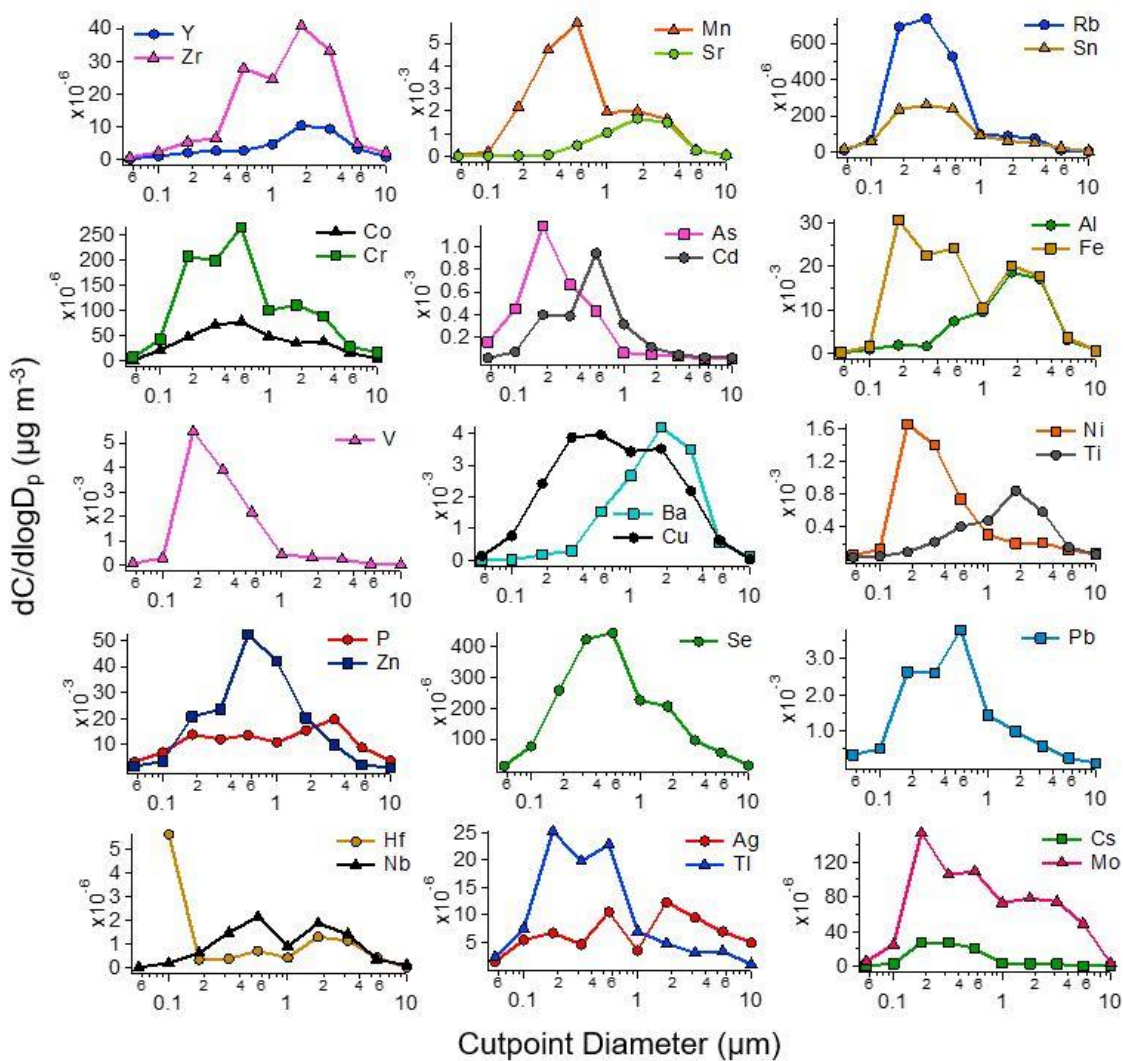
1382
 1383 **Figure 5.** Average mass size distribution of water-soluble ions speciated via IC in addition to
 1384 potassium from ICP-QQQ analysis.
 1385

1386



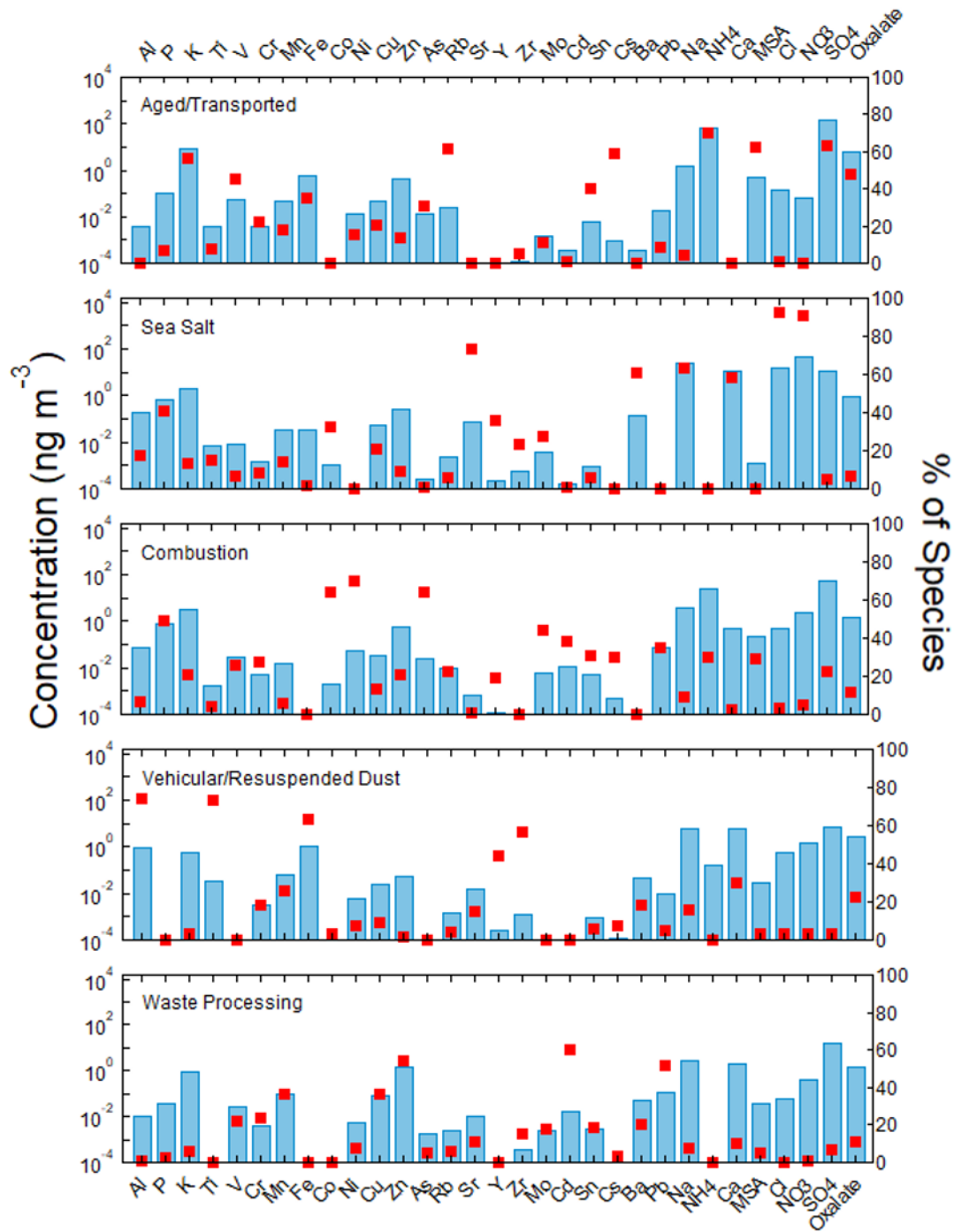
1387
1388
1389
1390
1391

Figure 6. Same as Figure 4, but for different supermicrometer aerodynamic diameter ranges sampled by the MOUDI: (a) 1.0–1.8 μm , (b) 1.8–3.2 μm ; (c) 3.2–5.6 μm , (d) 5.6–10 μm , (e) 10–18 μm , (f) > 18 μm .

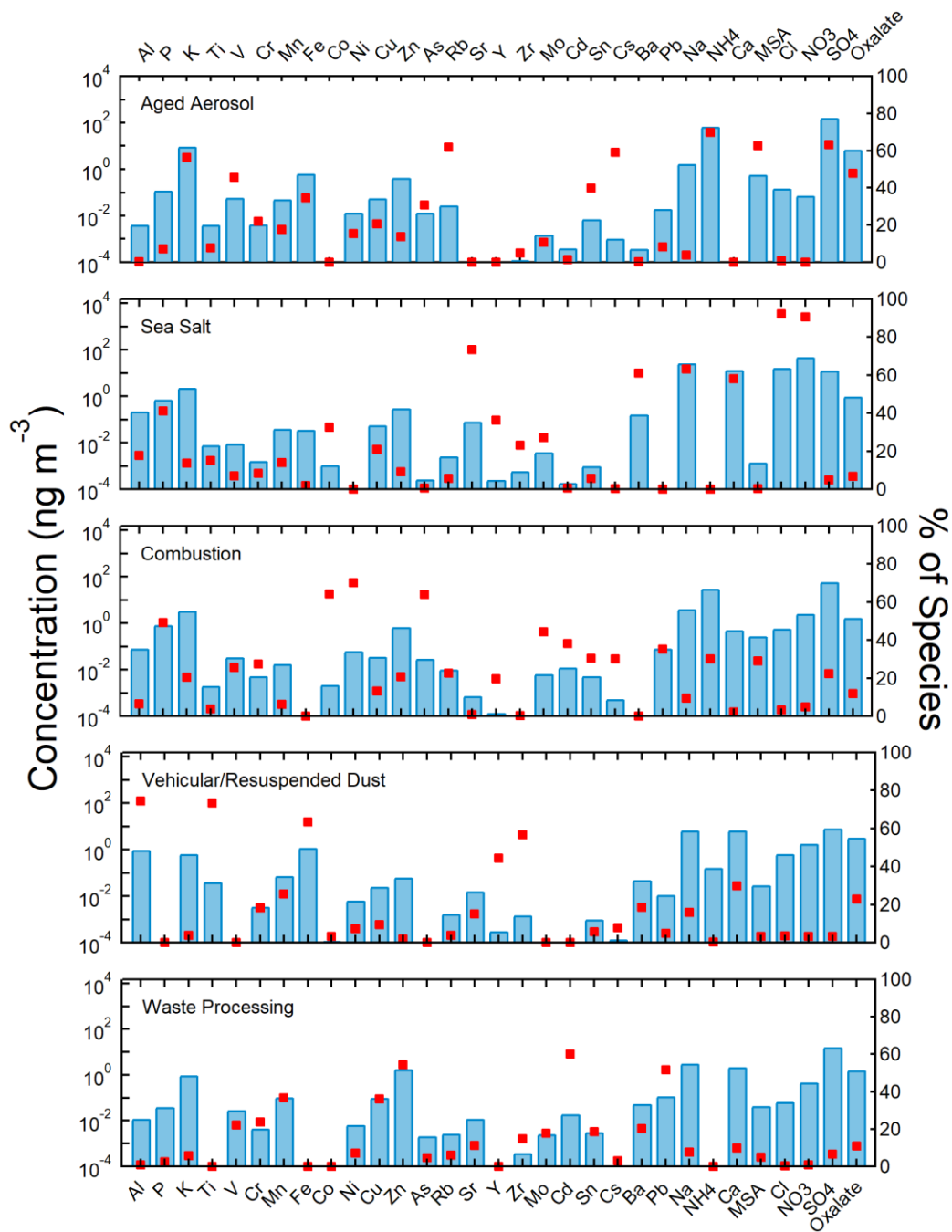


1392
 1393
 1394
 1395

Figure 7. Average mass size distribution of water-soluble elements speciated via ICP-QQQ.

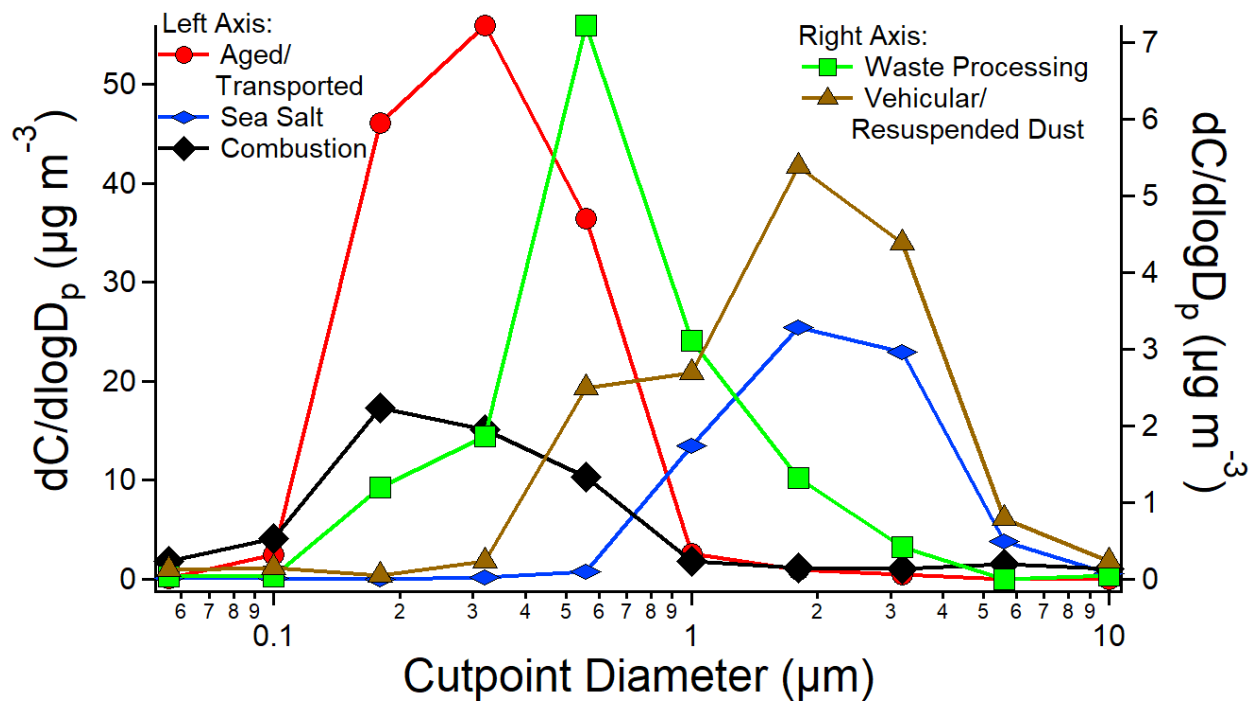


1396



1397
 1398
 1399
 1400
 1401

Figure 8. Overview of the PMF five factor solution with blue bars representing mass concentrations and red squares signifying the percentage of mass concentration contributed to constituents by each source factor.



1402
1403
1404

Figure 9. Reconstructed mass size distributions using PMF for the five major source profiles.